Phylogenomic Discordance in the Eared Seals is best explained by Incomplete Lineage Sorting following Explosive Radiation in the Southern Hemisphere

Running title: **Phylogenomics of Fur Seals and Sea Lions**

Authors: Fernando Lopes[1,2*], Larissa R. Oliveira[2,3], Amanda Kessler[1], Yago Beux[1], Enrique Crespo[4], Susana Cárdenas-Alayza[5], Patricia Majluf[5], Maritza Sepúlveda[6], Robert L. Brownell Jr.[7], Valentina Franco-Trecu[8], Diego Páez-Rosas[9], Jaime Chaves[10], Carolina Loch[11], Bruce C. Robertson[12], Karina Acevedo-Whitehouse[13], Fernando R. Elorriaga-Verplancken[14], Stephen P. Kirkman[15], Claire R. Peart[16], Jochen B. W. Wolf[16], Sandro L. Bonatto[1*]

[1] Escola de Ciências da Saúde e da Vida, Pontifícia Universidade Católica do Rio Grande do Sul, 90619-900 Porto Alegre, RS, Brazil

[2] Laboratório de Ecologia de Mamíferos, Universidade do Vale do Rio dos Sinos, São Leopoldo, RS, Brazil

[3] GEMARS, Grupo de Estudos de Mamíferos Aquáticos do Rio Grande do Sul, 95560-000 Torres, RS, Brazil

[4] CONICET, Centro Nacional Patagónico - CENPAT, Puerto Madryn, Argentina

[5] Centro para la Sostenibilidad Ambiental, Universidad Peruana Cayetano Heredia, Lima, Peru

[6] Centro de Investigación y Gestión de Recursos Naturales (CIGREN), Facultad de Ciencias, Universidad de Valparaíso, Valparaíso, Chile

[7] National Oceanic and Atmospheric Administration, NOAA, La Jolla, United States of America

[8] Departamento de Ecología y Evolución, Facultad de Ciencias, Universidad de la República, Montevideo, Uruguay

[9] Colegio de Ciencias Biológicas y Ambientales, COCIBA, Universidad San Francisco de Quito, Quito, Ecuador

[10] Department of Biology, San Francisco State University, 1800 Holloway Ave, San Francisco, CA, US

[11] Sir John Walsh Research Institute, Faculty of Dentistry, University of Otago, Dunedin, New Zealand

[12] Department of Zoology, University of Otago, Dunedin, New Zealand

[13] Unit for Basic and Applied Microbiology, School of Natural Sciences, Universidad Autónoma de Querétaro, Querétaro, Mexico

[14] Instituto Politecnico Nacional, Centro Interdisciplinario de Ciencias Marinas, La Paz, Mexico

[15] Department of Environmental Affairs, Oceans and Coasts, Cape Town, South Africa

[16] Division of Evolutionary Biology, Ludwig-Maximilians-Universität München, Münich, Germany

Corresponding authors (*): *slbonatto@pucrs.br; fernando.lopes@edu.pucrs.br*

Keywords: Phylogenomics, ILS, hybridization, Pliocene, Pleistocene, monophyly

ABSTRACT

The phylogeny and systematics of fur seals and sea lions (Otariidae) have long been studied with diverse data types, including an increasing amount of molecular data. However, only a few phylogenetic relationships have reached acceptance because of strong gene-tree species tree discordance. Divergence times estimates in the group also vary largely between studies. These uncertainties impeded the understanding of the biogeographical history of the group, such as when and how trans-equatorial dispersal and subsequent speciation events occurred. Here we used high-coverage genome-wide sequencing for 14 of the 15 species of Otariidae to elucidate the phylogeny of the family and its bearing on the taxonomy and biogeographical history. Despite extreme topological discordance among gene trees, we found a fully supported species tree that agrees with the few well-accepted relationships and establishes monophyly of the genus *Arctocephalus*. Our data support a relatively recent trans-hemispheric dispersal at the base of a southern clade, which rapidly diversified into six major lineages between 3 to 2.5 Ma. *Otaria* diverged first, followed by *Phocarctos* and then four major lineages within *Arctocephalus*. However, we found *Zalophus* to be non-monophyletic, with California (*Z. californianus)* and Steller sea lions (*Eumetopias jubatus*) grouping closer than the Galapagos sea lion (*Z. wollebaeki*) with evidence for introgression between the two genera. Overall, the high degree of genealogical discordance was best explained by incomplete lineage sorting resulting from quasi-simultaneous speciation within the southern clade with introgresssion playing a subordinate role in explaining the incongruence among and within prior phylogenetic studies of the family.

INTRODUCTION

For some time, it was widely accepted that by increasing the volume of molecular data even simple phylogenetic methods would unravel the true phylogenetic history of species (Rokas et al. 2003; Faircloth et al. 2013; Hoban et al. 2013; McCormack and Faircloth 2013). However, studies using whole genome data have found that inference of the true species tree, if such a tree exists, may be extremely challenging for some parts of the tree of life (Nakhleh 2013). These difficulties stem from a high degree of genealogical discordance among genomic fragments (GF) trees estimated from partitioned genomic data (e.g., genes or independent genomic fragments) (Peter 2016; Harris and DeGiorgio 2016; Elworth et al. 2018; Jones 2019).

Theoretical and empirical studies have shown that genealogical incongruences have three leading causes: incorrect estimation of the gene trees (e.g., caused by insufficient phylogenetic information, incorrect model specification or intralocus recombination); incomplete lineage sorting (ILS), found when ancestral polymorphism is persistent between successive speciation events (see Maddison and Knowles 2006; Oliver 2013); and introgression between lineages (hybridization) (e.g., Rheindt et al. 2014; Figueiró et al. 2017; Zhang et al. 2017). While technical issues as in the first problem could, in theory, be resolved, the latter two reflect the biological reality of evolutionary independence among recombining, genomic fragments (Hudson 1983; Griffiths and Marjoram 1997). Most methods used to estimate species trees assume only ILS, ignoring the consequences of hybridization for phylogenetic reconstruction (Stamatakis 2014; Drummond and Bouckaert 2015). Despite recent progress in developing models that include introgression, such as the so-called multispecies network models (e.g., Leaché et al. 2014; Wen and Nakhleh 2018), they continue to present several limitations, in particular when dealing with more than a few species (Degnam 2018). Consequently, resolving relationships among species that radiated

93 rapidly and putatively underwent both ILS and hybridization has proven challenging
94 (Chakrabarty et al. 2017; Esselstyn et al. 2017; Reddy et al. 2017).

95 The difficulty in establishing phylogenetic consensus (see below) and evidence for
96 current hybridization (Lancaster et al. 2006) make the otariids a compelling test case to assess
97 the relative impact of ancestral polymorphism and introgression on phylogenetic
98 reconstruction during rapid diversification. There are 15 extant species of fur seals and sea
99 lions within the Otariidae (Berta et al. 2018) with some uncertainty regarding the taxonomic
100 status of species such as *Arctocephalus philippii* and *A. townsendi* (see Committee on
101 Taxonomy of the Society for Marine Mammalogy 2020 for details, see Repenning et al.
102 1971; Yonezawa et al. 2009; Berta and Churchill 2012; Churchill et al. 2014, Berta et al.
103 2018). The initial diversification of the main lineages of Otariidae occurred around 11
104 (Yonezawa et al. 2009) to 9 Ma (Berta et al. 2018, Nyakatura and Bininda-Emonds 2014, this
105 study). On the other hand, species in the disputed genus *Arctocephalus* (see below) emerged
106 during a near-simultaneous succession of cladogenetic events within less than 0.5 Ma (Berta
107 et al. 2018; this study) corresponding to approximately 2.5 *Ne* generations (estimated from
108 data in Suppl. Table 3 of Peart et al. 2020). During such a short period, lineage sorting is
109 expected to be incomplete (Hudson et al. 2003; Rosenberg et al. 2003; Mugal et al. 2020)
110 with putative events of hybridization occurring, which makes this group particularly suited to
111 investigate the underpinnings of gene tree species tree discordance.

112 Otariids occur in the North Pacific Ocean and Southern Hemisphere and are found from
113 tropical waters in the eastern Pacific to polar regions (Churchill et al. 2014; Berta et al. 2018).
114 Although the systematics and phylogeny of the family have been extensively studied for over
115 100 years (Sclater 1897; Scheffer 1958; Wynen et al. 2001; Deméré et al. 2003; Árnason et
116 al. 2006; Yonezawa et al. 2009; Berta and Churchill 2012; Nyakatura and Bininda-Emonds
117 2012; Churchill et al. 2014; Berta et al. 2018), several relationships, in particular those within
118 *Arctocephalus*, the most diverse (eight species) otariid genus, remain unclear (Yonezawa et

al. 2009; Berta and Churchill 2012). For example, older studies based on morphology suggested grouping the fur seals (*Callorhinus ursinus* and *Arctocephalus* spp.) in the Arctocephalinae, which are characterized by small body size and thick pelage, and the sea lions in the Otariinae, which are characterized by larger body size and reliance on blubber rather than fur for thermal insulation (Berta and Demeré 1986; see review in Berta et al. 2018). However, more recent studies that used a combination of a few mitochondrial or nuclear genes and morphological data did not support these subfamilies (e.g., Yonezawa et al. 2009; Berta and Churchill et al. 2012; Churchill et al. 2014; Nyakatura and Bininda-Emonds 2014; Berta et al. 2018). Most of these phylogenies grouped the Southern Hemisphere otariids (i.e., *Otaria*, *Neophoca, Phocarctos*, and *Arctocephalus*) in the so-called southern clade, which is considered the sister clade of the sea lions of the Northern Hemisphere (i.e., *Zalophus* and *Eumetopias*) (Yonezawa et al. 2009, Churchill et al. 2014).

Another major difference between studies concerns the monophyly of *Arctocephalus*. A combined phylogeny produced by analyzing published morphological and molecular data reported *Arctocephalus sensu lato* as paraphyletic (Berta and Churchill 2012), restricting the genus to the type species *Arctocephalus pusillus*, and assigning the remaining species to *Arctophoca*. Other authors proposed that the use of *Arctophoca* was premature because of the remaining uncertainties surrounding the phylogenetic relationships in the group (e.g., Nyakatura and Bininda-Emonds 2014). Subsequently, the Committee on Taxonomy of the Society for Marine Mammalogy, which initially supported the proposal of Berta and Churchill (2012), adopted the conservative use of *Arctocephalus sensu lato* for all southern fur seals pending further studies (Committee on Taxonomy 2020). In short, there seemed to be no two identical phylogenies for the family and no explanation for the high level of discordance between studies.

The divergence times and biogeography within the Otariidae also present uncertainties, given the disagreement between studies. The most recent biogeographical

studies (e.g., Yonezawa et al. 2009; Churchill et al. 2014) agree on a North Pacific origin for Otariidae and support the hypothesis of one primary trans-equatorial dispersal event into the eastern South Pacific Ocean, that gave rise to the Southern Hemisphere clade (see Churchill et al. 2014). It has been estimated that this dispersal event and the diversification of the southern clade occurred at ~7 - 6 Ma (Yonezawa et al. 2009, Churchill et al. 2014, Berta et al. 2018). The more recent diversification within *Arctocephalus* may have occurred 4-3 Ma (Nyakatura and Bininda-Emonds 2012) or as recently as <1 Ma (Berta et al. 2018).

In this study, we used whole genome sequence data to investigate the phylogenetic relationships and estimate the divergence times of Otariidae species. We used several phylogenomic approaches, including multispecies coalescent models, to clarify most of the unresolved issues in the evolutionary history of Otariidae. We also investigated the main factors responsible for the high level of topological incongruences within the family, finding they were caused by rampant incomplete lineage sorting and some introgression events.

MATERIAL AND METHODS

Sample Collection and Genome Sequencing

Skin samples from nine otariid species (Table 1) were collected from live or fresh carcasses found ashore. Piglet ear notch pliers were used to extract ~0.5 cm^3 skin samples. The samples were stored in ethanol 70% and cryo-preserved at -20 ºC. Genomic DNA extractions were carried out with DNeasy Tissue Kit (Qiagen) following the manufacturer's protocol.

We sequenced the whole genome of one individual from seven species of *Arctocephalus* and two other monospecific genera (*Phocarctos* and *Otaria*) (Table 1 and Supplementary Table S1 available on Dryad at https://doi:10.5061/dryad.pzgmsbchw). Genomic libraries were prepared with Illumina DNA PCR-free or TruSeq Nano kits with an

insert size of 350 bp, and two libraries were sequenced (PE150) per lane on the Illumina HiSeq X platform. Raw genome reads from *Arctocephalus gazella*, *Zalophus wollebaeki*, *Zalophus californianus*, *Eumetopias jubatus*, and *Callorhinus ursinus* (Table 1 and Supplementary Table S1) were retrieved from the NCBI Sequencing Read Archive (https://www.ncbi.nlm.nih.gov/sra). We used the genome of the walrus, *Odobenus rosmarus* (ANOP00000000 - Foote et al. 2015) as the reference for mapping and as the outgroup for most analyses. Since we had already started several analyses before genome-wide data from *C. ursinus*, *E. jubatus*, and *Z. californianus* were available, we did not include them in some less critical but time-consuming analyses.

Our study included 14 of the 15 extant Otariidae species (all *Arctocephalus*, *Phocarctos*, *Otaria*, *Zalophus*, *Eumetopias*, and *Callorhinus*). *Neophoca cinerea* was not included in our study. However, its position as the sister species of *P. hookeri* is uncontentious (see Yonezawa et al. 2009; Berta and Churchill 2012; Nyakatura and Bininda-Emonds 2012; Berta et al. 2018).

Sequencing quality control was performed using FastQC (Andrews 2010). Reads were trimmed for vestigial adapters, mapped against the *O. rosmarus* genome and locally realigned using the bam_pipeline implemented on PALEOMIX 1.2.13.2 (Schubert et al. 2014). Reads with length-size <100 bp and Phred-score <30 were filtered out by AdapterRemoval v2 (Schubert et al. 2016); the remaining paired-end reads were mapped using BWA 0.7.17 (Li and Durbin 2009) and the -mem algorithm. Paired-end reads with mapping quality Phred-score <20, unmapped reads and single-reads were discarded from the downstream pipeline and reads that were sequenced more than two or less than one standard deviations from the average of coverage of each genome (Supplementary Table S2) were not used in the analyses (Arnold et al. 2013; Gautier et al. 2013). PCR duplicates were detected and removed by Picard Tools 2.18.5 (broadinstitute.github.io/picard/), and miscalling indels were locally realigned by GATK 3.8 (McKenna et al. 2010).

196

197 *Consensus, Alignments and SNP Calling*

198 Consensus sequences of all genomes were generated with ANGSD 0.921 (Korneliussen
199 et al. 2014) using the parameters *doFasta 2, doCounts1,* and *explode 1*. Single-nucleotide
200 polymorphisms (SNPs) were called following the filters: *uniqueOnly 1*, *remove_bads 1*,
201 *only_proper_pairs 1*, *C 50*, *baq 1*, *setMinDepth* 140, *setMaxDepth 1400*, *setMinDepthInd 5*,
202 *setMaxDepthInd 100*, *doCounts 1*, *GL 1*, *doMajorMinor 1*, *SNP_pval 1e-3*, *doGeno 32*,
203 *doPost 1*, *doPlink2*. After the SNP calling, a PLINK variant panel was converted to VCF
204 format with Plink 1.9 (Chang et al. 2015). The VCF file did not contain SNPs from the
205 walrus genome. We removed all information of repetitive, coding, and transposons present in
206 the General Feature Format File of *O. rosmarus* genome with BEDTools 2.27.0 maskfasta
207 option (Quinlan and Hall 2010).

208

209 *Phylogenetic Information, Phylogenomic Analyses, and Genealogical Discordance*
210 *Estimation*

211 We first estimated relationships between species using the full sequence data set. A
212 whole-genome maximum-likelihood (ML) tree was inferred with RAxML-NG-MPI (Kozlov
213 et al. 2019) directly from the SNP panel using the HKY substitution model inferred with
214 ModelTest-NG, 100 bootstrap replicates and *C. ursinus* as the outgroup. We also used the
215 VCF2Dis script (github.com/BGI-shenzhen) to estimate the p-distance matrix from the VCF
216 file, followed by a neighbor-joining tree with PHYLIP 3.697 (Felsenstein 1989).
217 Additionally, we estimated ML trees for each alignment of the ten largest scaffolds with
218 RAxML-HPC-PTHREADS 8.2 (Stamatakis 2014) using GTR+G (best-fit substitution model
219 as estimated by ModelTest-NG for all the largest scaffolds, Darriba et al. 2019) and 100
220 bootstrap replicates.

Next, we estimated phylogenies using smaller segments partitioning scaffolds into sets of smaller nonoverlapping genomic fragments (GFs) of 10, 20, 50, 80, 100, and 200 kilobases (kb) in length. To reduce the effect of linkage disequilibrium between GFs, they were separated by 100 kb, regardless of window size, following Humble et al. (2018) demonstrating low levels of linkage disequilibrium (r^2~0.05) at this physical distance in the Antarctic fur seal. Several filters were used: scaffolds smaller than the GF partition size were excluded; sites with more than 20% of missing data were removed with trimAl v1.4 (Capella-Gutierrez et al. 2009); alignments smaller than half of the original alignment size were also discarded. To reduce the effect of intra-fragment genetic recombination on the phylogenetic estimation, we used the software 3Seq on *full run mode* (Lam et al. 2017). We removed the alignments with evidence of recombination at a *p-value* <0.01 after Bonferroni correction (Rice 1989). To test the effect in quantification of the genealogical discordance (see below) of both the spacing of GFs by 100 kb and of the 3Seq filtering for recombination, we generated additionally datasets (only 50 kb GFs): with no 3Seq filtering (i.e. with all GFs) and without the 100 kb spacing (i.e. contiguous GFs).

To assess the amount of genetic information content on GFs, we randomly sampled 10,000 GFs of 50 kb and used the AMAS tool (Borowiec 2016) to count the number of parsimony-informative sites in these alignments and the number of differences between two closely related fur seals (*A. australis* and *A. galapagoensis*). Finally, we reconstructed ML trees with RAxML-HPC-PTHREADS 8.2 for each GF that passed by the mentioned filters in all GF partitions (10 to 200 kb) using the same parameters as above.

To quantify the genealogical discordance throughout genomes, we counted the frequency of each topology with Newick Utilities 1.1 (Junier and Zdobnov 2010) for each set of GF trees by using the sub-programs nw_topology and nw_order in a pipeline. We also estimated the gene concordance factor (gCF) and the site concordance factor (sCF) (Minh et al. 2018) implemented in IQ-TREE 1.7 (Nguyen et al. 2015) as a complement to standard

measures of branch support (in this case bootstrap) and to quantify the disagreement among loci and sites in our phylogenomic dataset. The gCF is the percentage of decisive GF trees showing a particular branch from a species tree, while sCF is the percentage of decisive alignment sites supporting a branch in the reference tree when individual gene alignments are relatively uninformative (Minh et al. 2018). The estimation of gCF and sCF followed three steps. First, in IQ-TREE, the species phylogeny used as reference was recovered based on all (10,806) GFs of 50 kb concatenated, the edge-linked proportional partition model and 1,000 replicates of ultrafast bootstraping. Second, using a maximum-likelihood approach and substitution models inferred for each locus, GF trees were estimated from each genomic fragment. Then, gCF and sCF were computed across all nodes of the generated species tree and GF trees. The outputs were visualized with the support of the R script available on http://www.robertlanfear.com/blog/files/concordance_factors.html

Species Tree Estimation

Two methods were used to reconstruct the species tree from multiple GF trees. First, all GFs ML trees were used to estimate a maximum quartet support species tree with the multispecies coalescent model (MSC) of ASTRAL-III (Zhang et al. 2018) by applying the exact search method. Second, we estimated the species tree and divergence times with the Bayesian Inference method StarBEAST2 implemented in the BEAST 2.5.2 package (Rambaut and Drummond 2010; Bouckaert et al. 2014; Ogilvie et al. 2017). Since this Bayesian analysis is very time-consuming and the ASTRAL species trees of all GF datasets, except the 10 kb GF, were identical (see Results), we used 300 randomly selected GFs from the 50 kb dataset. The main priors used were: linked clock models, constant population sizes, the HKY substitution model with empirical base frequencies, an estimated six gamma categories site model, and the Yule Tree model. To estimate divergence times, we used a strict molecular clock as a prior with a lognormal distribution and a standard mammalian

genomic mutation rate of 1×10^{-8} bp^{-1} gen^{-1} (Kumar and Subramanian 2001; Peart et al. 2020), with a large standard deviation of 0.4 (5% and 95% quantiles of 4×10^{-9} and 4×10^{-8} bp^{-1} gen^{-1}, respectively) to account for other rates found in the literature. We assumed a generation time of 10 years based on generation time estimates published by the IUCN (IUCN, 2017) as compiled in Peart et al. (2020) for a subset of the species considered here. We also added two calibration points in the phylogeny. One was at the origin of the *Arctocephalus* spp. clade, based on the age of the oldest *Arctocephalus* fossil record (*Arctocephalus* sp. nov. - Varswater Formation of South Africa), which constrained the origin of this group to a lower bound of 2.7 Ma (Avery and Klein 2011), since the incomplete and imperfect nature of the fossil records only provides evidence for the minimum age of a clade (Benton and Ayala 2003). The second was the date of the root, which we set as a normal prior with a mean of 20 Ma (± 3.0) in the divergence between Otariidae and Odobenidae (Yonezawa et al. 2009; Nyakatura and Bininda-Emonds 2012). We ran a Bayesian Markov Chain Monte Carlo (MCMC) of 500,000,000 steps sampled each 20,000 with a burn-in of 10%. To test underestimation of the internal branches due to possible undetected hybridizations (Leaché et al. 2014, Elworth et al. 2019), we also estimated a StarBEAST2 species tree using only the GFs of 50 kb whose ML tree topology was identical to our main species tree (see results) using the same parameters as above. We checked the MCMC runs with Tracer 1.7 (Rambaut and Drummond 2007).

As an additional estimation of divergence times, the species tree topology (recovered by ASTRAL-III and StarBEAST2) was used as input in the Bayesian species tree estimation of the BP&P program (Ziheng 2015; Flouri et al. 2018). We used the same 300 GFs of 50 kb applied in the initial StarBEAST analysis, and the following parameters: an MCMC chain of 2,000,000 replicates with burn-in of 200,000, a theta prior of 0.01 and a tau prior of 0.02. The theta prior specifies the inverse-gamma prior, the number of differences per kb, and the tau specifies the divergence time parameter for the root. For this analysis, the divergence times

were calibrated based on the age of the root as above (Yonezawa et al. 2009; Nyakatura and Bininda-Emonds 2012). All trees were visualized and edited for clarity on FigTree 1.4.4 (Rambaut 2017) or Dendroscope 3 (Huson and Scornavacca 2012).

Simulation of Genomic Fragments Trees from Assuming a Known Species Tree

To test if the high level of topological discordances between trees from the GFs could be explained by ILS alone, we simulated 10,000 GF trees under a multispecies coalescent framework implemented in the function sim.coaltree.sp in the R phylogenetic package Phybase (Liu and Yu 2010). As input for the simulations, we used our species tree as estimated by StarBEAST2, which besides the topology, also estimated the branch lengths and effective population sizes (*dmv* parameter in the StarBEAST2 species tree) for all internal and terminal branches. Note that both the estimation of the species tree by StarBEAST2 and the GF trees simulated allowed the occurrence of ILS. We then tabulated the frequency of the tree topologies and calculated the linear Pearson's correlation between the simulated and empirical frequency distribution (following Wang et al. 2018).

Mitochondrial Genome Phylogeny

We obtained the mitochondrial genomes of the fur seals and sea lions by mapping all reads with PALEOMIX 1.2.13.2, using the parameters reported above for the nuclear genomes, against a mitochondrial genome (mtDNA) available on GenBank (*A. townsendi* - NC008420). In order to validate the recovered mtDNAs, we assembled and aligned the generated sequences with those published on GenBank. After the alignment step, the mitochondrial control region was excluded. An mtDNA Bayesian phylogenetic tree was estimated with BEAST 2.5.2 package with the parameters: Yule Tree Model prior; GTR substitution model with four gamma categories (estimated with ModelTest-NG); and the

Uncorrelated Lognormal Clock Model with lognormal distribution with a mean substitution rate of 2% site^{-1} million year^{-1} (Nabholz et al. 2007) and a standard deviation of 0.8.

Introgression Between Species

Within the Dsuite package, we used the program Dtrios (Malinski 2019) and jackknife blocks to infer *D* statistics (also called ABBA-BABA test). This analysis compares the distribution of ancestral (A) and derived (B) sites in a four-taxa asymmetric phylogeny (((P1, P2), P3), O) with P1 to P3 being ingroups and O being the outgroup. Under the null hypothesis that P1 and P2 descend from an ancestor that diverged at an earlier time from the ancestral population of P3, derived alleles B should be found equally often in P1 and P2. Consequently, GF trees following allelic ABBA or BABA relationships should be equally likely for incompletely sorted ancestral polymorphism. Gene flow between P2 and P3 will lead to an excess of ABBA patterns reflected in a positive *D*-statistic, gene flow between P1 and P3 to a surplus of BABA patterns reflected in a negative *D*-statistic (Durand et al. 2011). In the Dsuite package, P1 and P2 are ordered so that nABBA >= nBABA and, consequently, is never negative. Statistical significance for a deviation of the *D*-statistic from zero was assessed by calculating Z-scores and their associated p-values by the standard block-jackknife procedure (Durand et al. 2011), using p-value < 0.05 as an indication for a possible signal of introgression. To take into account the multiple testing problem, the p-values were adjusted by the Bonferroni correction (Malinski 2019). The Dtrios program orders each trio of taxa by assuming that the correct tree is the one where the BBAA pattern is more common than the discordant ABBA and BABA patterns, which are assumed to be introgressed loci.

We also estimated the f_3 and f_4-statistics (Patterson et al. 2012) in threepop and fourpop modules, respectively, of *TreeMix* package (Pickrell and Pritchard 2012; Harris and DeGiorgio 2016). The f_3-statistics explicitly tests whether a taxon of interest *C* is the result of admixture between two other taxa *A* and *B* considering the product of allelic differentials

between populations (c-a)(c-b): negative values suggest that allele frequencies c are intermediate at many positions, which is consistent with a history of admixture while positive values are not evidence against admixture. F_4-statistics use unrooted four-population phylogenies to visualize shared genetic drift among taxa. For a f_4 ((A,B),(C,D)) topology without invoking admixture the allele frequency difference between A and B (a-b) and between C and D (c-d) should be unrelated and hence results in f_4 =((a-b)(c-d))= 0. A significantly positive f_4 implies gene flow between A and C, or B and D. Otherwise, a significantly negative value implies gene flow between A and D, or B and C. Significant f_4 values may also be interpreted as a rejection of the given topology (Peter 2016; Zhenge and Janke 2018). The significance of f_3 and f_4-statistics is based on the Z-score and was calculated over 872 jackknife blocks of 50,000 SNPs. Significantly positive (Z > 3) and significantly negative (Z < -3) values, after Bonferroni correction, reject the null hypothesis. We plotted the distribution of f_4-values with the function f4stats from admixturegraph (Leppälä et al. 2017), an R package.

We also used the newly developed QuIBL approach (Quantifying Introgression via Branch Lengths - Edelman et al. 2019), a statistical framework to estimate the number of discordant loci in a set of GF trees that reflect introgression events or ILS alone. Unlike *D* and *f*-statistics, a QuIBL analysis does not rely on topology imbalances but instead uses the distribution of internal branch lengths and calculates the likelihood that the discordant GF tree for a given region is due to introgression rather than ILS (Edelman et al. 2019). To distinguish whether the regions with local topologies discordant from the species tree were more likely to introgression or ILS, we used a Bayesian information criterion (BIC) test with a strict cutoff of dBIC <-10 to accept the ILS+introgression model as a better fit for the data, as suggested by the authors (Edelman et al. 2019). For this analysis, we used the GF trees generated from the partition of 50 kb. Since the analysis with 15 taxa (14 Otariidae plus *Odobenus*) is time-consuming, we used every other topology (5,454 GF trees) from the full

dataset of 10,908 topologies. We used *O. rosmarus* as outgroup and our species tree estimated above with QuIBL default parameters as recommended by the authors (Edelman et al. 2019).

RESULTS

Fourteen sequenced otariid genomes, including nine fur seals and five sea lion species (Table 1), were mapped on the walrus genome with an average coverage of 27.79X (± 12.07X) (see Supplementary Table S2). The largest scaffold was 231.63 million bases (Mb), and the ten largest scaffolds summed-up to around 1.5 Gb, ~62% of the reference genome (2.4 Gb). Repetitive regions in the reference genome were masked in the consensus genomes (~40% of the reference genome), resulting in a high-quality non-repetitive alignment of ~1.1 Gb for further analyses. After filtering (removing masked regions, missing data, genomic fragments (GFs) with less than 50% of the original information, and those with the signal of intra-locus recombination), we obtained between 14,075 (with 10 kb) and 5,701 (with 200 kb) GFs a minimum of 100 kb apart from each other for the GF trees analyses (Table 2).

The Bayesian species tree (estimated with StarBEAST2 using 300 GF of 50 kb) (Fig. 1), the ASTRAL-III species trees (from thousands of ML trees using GFs ranging from 20kb to 200 kb) (Supplementary Fig. S1), the ML trees of eight of the ten largest scaffolds (Supplementary Fig. S2), the ML whole-genome tree (Supplementary Fig. S3), and the NJ tree (estimated using the genetic distances among the whole genomes, Supplementary Fig. S4) all resulted in the same tree topology with high support for most or all branches, hereafter named as the Otariidae species tree.

This species tree strongly supports the existence of a Southern Hemisphere clade (see Churchill et al. 2014), the monophyly of the genus *Arctocephalus* and its close relationship to *P. hookeri* and *O. flavescens*. The clade of *Z. californianus* + *E. jubatus* + *Z. wollebaeki,*

Northern species with the southernmost range reaching the equator, was more distantly related to the Southern clade. *C. ursinus*, also a Northern hemispheric species, is sister to all other otariids (Fig. 1b). Surprisingly, *E. jubatus* and *Z. californianus* grouped as sister species, and *Z. wollebaeki* as sister to them. Within *Arctocephalus*, there were four main lineages: *A. pusillus* + *A. tropicalis; A. phillippii* + *A. townsendi; A. gazella* and the clade comprised of *A. forsteri* + *A. galapagoensis* + *A. australis* (Fig. 1b). Only three alternative topologies were found in these analyses, one in which *P. hookeri* and the *A. tropicalis* + *A. pusillus* clade switched position (ASTRAL-III with GFs 10 kb, Supplementary Fig. S1) and two in which *A. gazella* was found at two different positions within *Arctocephalus* (found in two ML scaffold trees) (Supplementary Fig. S2).

The phylogeny of the mitochondrial genomes (Supplementary Figs. S5 and S6) was similar to the species tree, with high posterior probabilities for most nodes and only two differences: (1) the switched position between *P. hookeri* and the *A. tropicalis* + *A. pusillus* clade, as in the ASTRAL species tree of 10 kb GFs, and 2) the sister relationship of *A. australis* with *A. forsteri*, instead of with *A. galapagoensis*. The time scales differ, the mtDNA phylogeny divergences were more recent, especially for *C. ursinus* and the northern clade, and the southern clade diversification would have started ~2 Ma and did not occur as rapidly as found in the nuclear genome species tree.

The species tree divergence times estimated with StarBEAST2 and BP&P were very similar (Fig. 1b and Supplementary Fig. S7). The divergence between walrus and the Otariidae was 19.4 Ma (95% confidence interval (CI) = 17.2 - 23.2 Ma), and within the Otariidae, *C. ursinus* diverged ~9.1 Ma (95% CI = 8.1 – 10.9 Ma) followed by the clade *Z. wollebaeki* + *Z. californianus* + *E. jubatus* at 5.4 Ma (95% CI = 4.8 - 6.4 Mya). After that, around the Pliocene to Pleistocene transition, six lineages diverged almost simultaneously (between ~3 and 2.5 Ma), originating in order: *O. flavescens*, *P. hookeri*, and the four main *Arctocephalus* lineages described above. Specifically, *Arctocephalus* diversification began

~2.8 Ma (95% CI = 2.5 - 3.3), the divergence times between *A. pusillus* + *A. tropicalis* and between *A. forsteri* + *A. australis* + *A. galapagoensis* were very similar at, ~1.2 Ma (95% CI = 1.0 - 1.4 and 1.0 - 1.5, respectively). The two groups that diverged more recently were *A. phillippii* + *A. townsendi* and *A. australis* + *A. galapagoensis*, at 0.6 and 0.5 Ma, respectively (95% CI = 0.5 - 0.7 and 0.4 - 0.6). The most recent divergence occurred between *Z. wollebaeki*, *Z. californianus*, and *E. jubatus* ~0.25 Ma (95% CI = 2.1 – 3.1). The main difference between StarBEAST2 and BP&P results was that in the latter, the divergence of *A. gazella* was almost simultaneous with that of *A. forsteri* (~1.2 Ma, Fig. 1 and Supplementary Figure S7).

Finally, we evaluated whether the almost simultaneous divergence time for the six lineages estimated in our species tree could be an artifact caused by the underestimation of divergence times (shortening of internal branch lengths) in methods that do not account for introgression (Elworth et al. 2019). In this context, we estimated a new StarBEAST2 calibrated species tree using only the 113 GFs of 50 kb whose ML tree topologies were identical to the species tree. The divergence times of this tree were almost identical to the 300 GFs species tree, in particular, the six nodes related to the explosive radiation (Supplementary Fig. S7), suggesting these very short divergence times were not artifacts of unaccounted hybridizations (see discussion).

Genome Fragment Information Content and Phylogenetic Discordance

When the ML phylogeny of each GF was estimated separately, we found thousands of different topologies in each GF dataset (Supplementary Fig. S8); most occurred just once or a few times (that is, were estimated from one or a few GFs). The most frequent topology in the 10 kb dataset occurred in only 45 of the 14,012 GFs (i.e., in ~0.4% of the GF, Table 2). Although the frequency of the most common topology in each dataset proportionally increased with the size of the GFs (from 10 to 200kb), the most common topology only

453 comprised ~3.8% of all topologies in even in the 200 kb data set (Table 2 and Supplementary
454 Fig. S8). A very similar pattern was obtained for the alternative datasets with no filtering for
455 recombination and without the 100 kb spacing between GFs (Supplementary Table S3). The
456 Otariidae species tree was the most frequent topology in all datasets except for the 10 kb GF.
457 Information content was high for all GF size classes. Considering the 50 kb GF as an
458 example, the mean variable sites between the two closest species (*A. australis* and *A.*
459 *galapagoensis*) was ~40, and the mean number of parsimony informative sites in the
460 alignments ~200 (Supplementary Fig. S9) yielding enough variation to estimate reliable GF
461 trees.

462 The IQ-TREE analysis recovered the same species tree topology with the highest
463 branch support (100) for all nodes (Supplementary Fig. S10). However, the four nodes (nodes
464 16, 17, 19 and 20) that define the relationships between the six main lineages of the southern
465 clade that arose almost simultaneously presented very low gene concordance (gCF: 19.9 -
466 32.2) and site concordance (sCF: 39.2 - 43.7) factors (Supplementary Fig. S9). In contrast,
467 the other nodes showed much higher values for both statistics. Furthermore, less than 33% of
468 the 10,806 GF trees supported the species tree for those nodes, but >76% supported the
469 remaining nodes (Fig. 2).

470

471 *Hybridization vs. Incomplete Lineage Sorting*

472 We used *D* (ABBA-BABA test), *f3*, and *f4*-statistics to investigate whether there is
473 evidence of past events of hybridization (genomic introgression) between the species and if
474 these events could explain the high level of topological discordance found in the southern
475 clade. No evidence of introgression was found in the f_3-statistics as all values were positive
476 (not shown). For the ABBA-BABA test, a few *D*-statistics were significant ($p < 0.05$), but all
477 turn out non-significant after Bonferroni correction (not shown). Otherwise, f_4-statistics
478 identified many significant (even after Bonferroni correction) sets of shared drift pathways

between the species (Supplementary Figs. S11 and S12) that could be interpreted as signals of introgression or as supporting an alternative (to the species tree) phylogenetic relationship between the species considered (Peter 2016; Zhenge and Janke 2018). The strongest signals ($f_4 > 0.01$) supported introgression between *A. australis* and *A. forsteri*. The other significant f_4 values were very small ($f_4 < 0.001$, Supplementary Figs. S11 and S12). Note that except for the tests that support introgression between *A. australis* and *A. forsteri* (Supplementary Fig. S11), all the other significant results could be interpreted as implying an alternative phylogenetic relationship between the six lineages that diverged almost simultaneously within the southern clade (see above and Fig. 1, and Supplementary Fig. S7), that is, where the internal branches were extremely small. Therefore, we next used two approaches to test if the high level of GF trees discordance (see above) and these f_4-statistics results could be explained mostly by ILS, not introgression.

First, we used QuIBL analysis in distinguishing between ILS and introgression, which is thought to be more powerful than previous methods, such as f_4-statistics or the *D* statistics (Edelman et al. 2019). This method uses the distribution of internal branch lengths to calculate the likelihood that a given genome fragment shows its GF topology due to introgression rather than ILS. QuIBL suggested that ILS could explain almost all significant f_4 results in those clades that emerged almost simultaneously (Supplementary Table S3). It identified only three significant events of hybridization with similar intensities: between *A. forsteri* and the ancestor of *A. australis* and *A. galapagoensis*; between the ancestor of *A. philippii* and *A. townsendi* and *A. gazella*; and between *Z. wollebaeki* and the ancestor of *Z. californianus* and *E. jubatus* (Fig. 3).

Next, 10,000 GF trees were simulated using a multispecies coalescent model (that allows ILS but not introgression), whose parameters (the topology, divergence times, and effective population sizes) were those estimated by the StarBEAST2 species tree (Fig. 1).

The frequency distribution of the simulated GF tree topologies was similar to the observed distributions, in particular, for the 200 kb GFs partition (Supplementary Fig. S8). The simulation also presented the species tree as the most frequent topology (Table 2). The coefficient of correlation between the observed (50 and 200 kb data sets) and simulated distributions was 0.73 (Supplementary Fig. S13), which was high considering that the simulated topologies are true GF trees and are not affected by the uncertainties of the estimation as in the empirical dataset. These results suggest that the high level of GF tree discordance observed here could mostly be explained by ILS alone rather than by introgression events.

DISCUSSION

Otariidae Phylogenomics

We present the first whole genome species tree of the Otariidae, which consistently recovered a phylogeny with high support using several different approaches. Our phylogeny also resolved uncertainties still prevalent to date in this group, such as the monophyly of *Arctocephalus*. The only species for which we could not obtain a genome sequence was *Neophoca cinerea.* Although some recent molecular studies support that *N. cinerea* is sister to *P. hookeri* (e.g., Yonezawa et al. 2009; Nyakatura and Bininda-Emonds 2012), some have suggested that it may be positioned elsewhere (Deméré and Berta 2003) including a sister position to all Otariidae except *C. ursinus* (Churchill et al. 2014). Future integration of the *Neophoca* genome to the data presented here thus constitutes a critical step to fully resolve the phylogeny of the Otariidae.

Our results strongly support *C. ursinus* as a sister species to all other Otariidae, which was also supported by other phylogenetic studies (Wynen et al. 2001; Árnason et al. 2006; Yonezawa et al. 2009; Nyakatura and Bininda-Emonds 2012; Berta and Churchill 2012; Churchill et al. 2014), thoroughly refuting the validity of the subfamilies Arctocephalinae and Otariinae. It is noteworthy that, considering our whole-genome phylogenies and other recent

studies, *Callorhinus* diverged ca. 4 million years before the diversification of the rest of the family (Yonezawa et al. 2009; Boessenecker 2011; Nyakatura and Bininda-Emonds 2012; Berta et al. 2018).

Our study results offer robust support for the existence of the Northern Sea Lion clade, proposed by Churchill et al. (2014), consisting of *Zalophus* and *Eumetopias* (see Fig. 1). This Northern clade has been recovered in several previous studies (see Berta et al. 2018; Churchill et al. 2014; Berta and Churchill 2012; Yonezawa et al. 2009; Higdon et al. 2007; Árnason et al. 2006; Wynen et al. 2001), that also supported the monophyly of *Zalophus* (Wolf et al. 2007; Yonezawa et al. 2009; Churchill et al. 2014; Berta and Churchill 2012; Berta et al. 2018). Our analysis, however, recovered an unexpected but fully supported and close relationship between *E. jubatus* and *Z. californianus* with *Z. wollebaeki* as sister to them. It should be noted that most previous studies that support the monophyly of *Zalophus* used a few fragments of mtDNA (Yonezawa et al. 2009; Nyakatura and Bininda-Emonds 2012; Berta and Churchill 2012; Churchill et al. 2014, including the extinct Japanese sea lion - Wolf et al. 2007). Interestingly, the only study that used exclusively nuclear markers (AFLP data) found the same non-monophyletic relationship as found here (Dasmahapatra et al. 2009). If this relationship is supported by further studies, a taxonomy change would be necessary, such as synonymizing *Zalophus* with *Eumetopias*. The introgression we found between these species (see below) may help to explain their very recent divergence times and the very short internal branch separating *Z. wollebaeki* from the other two species (Fig. 1b). Together, our results motivate in-depth genomic-scale studies of this clade revisiting previous small-scale genetic studies of these species (Wolf et al. 2008; Schramm et al. 2009).

Previous authors had reached no consensus regarding the relationships between *Arctocephalus* spp., *P. hookeri*, *O. flavescens*, and *N. cinerea*, which has been called the southern clade (Churchill et al. 2014), except for a few subgroups within *Arctocephalus* (Berta et al. 2018). Our dated species trees showed that most of the speciation within the

557 southern clade was almost simultaneous (Fig. 1b), which could explain the high number of
558 different phylogenetic relationships found for this group to date. Our analyses based on
559 genome-wide data provide strong support for this clade, with the South American sea lion (*O.*
560 *flavescens*) being the first species to diverge around 3 Mya, followed by the New Zealand sea
561 lion (*P. hookeri*) and a monophyletic *Arctocephalus,* both at ~2.8 Mya. The genomic data and
562 the many different phylogenetic approaches we used support monophyly of *Arctocephalus*
563 and did not support the use of *Arctophoca* as first suggested by Berta and Churchill (2012).

564 Within *Arctocephalus*, four main lineages originated in fast succession between ~2.8
565 and 2.5 Ma. The first to diverge was *A. pusillus* + *A. tropicalis*. This position within
566 *Arctocephalus* for this clade was also found in several other recent studies (e.g., Berta et al.
567 2018), although some studies found it to have diverged before *Phocarctos* (e.g., Yonezawa et
568 al. 2009). The divergence time between the two species was ~1.2 Ma. The next clade to
569 diverge was the clade with *A. phillippii* + *A. townsendi*, with those species diverging more
570 recently at ~0.6 Ma. These results were expected since they were reported as sister species in
571 all previous molecular phylogenies (Yonezawa et al. 2009; Nyakatura and Bininda-Emonds
572 2012) and are morphologically very similar, with some authors still considering *A. townsendi*
573 a subspecies of *A. phillippii* (e.g., Committee on Taxonomy 2020 following Berta and
574 Churchill 2012). Considering the divergence time between these two species, which is similar
575 or older than that between *A. australis* and *A. galapagoensis*, and their geographic isolation,
576 we agree with most of the recent literature on their taxonomic status as full species
577 (Repenning et al. 1971; Higdon et al. 2007; Yonezawa et al. 2009; Nyakatura et al. 2012;
578 Aurioles-Gamboa 2015; Berta et al. 2018). The grouping of *A. gazella* with the *A. forsteri* +
579 *A. australis* + *A. galapagoensis* clade was found in some recent studies (e.g., Yonezawa et al.
580 2009; Churchill et al. 2014), although *A. gazella* was found in a polytomy with other
581 *Arctocephalus* species in most cases (e.g., Yonezawa et al. 2009; Berta et al. 2018) or in other
582 positions. Finally, the *A. forsteri* + *A. australis* + *A. galapagoensis* clade was also highly

583 expected, as these species were always closely related in previous phylogenetic studies and,
584 until around 1970s, these three taxa were considered conspecific (Reppening et al. 1971,
585 Brunner 2004). Nevertheless, there is a question over the species status of the New Zealand
586 fur seal (*A. forsteri*), that was also considered a subspecies under *A. australis* (see Berta and
587 Churchill 2012), and indeed, we found evidence of a low level of introgression between New
588 Zealand fur seal and the South American fur seal (see below). However, we support *A.*
589 *forsteri* as a full species based on the same arguments mentioned above for *A. phillippii* and
590 *A. townsendi*, also considering that they diverged from *A. australis* + *A. galapagoensis* more
591 than 1 Ma.

592 The placement of *P. hookeri* and *A. tropicalis* + *A. pusillus* were switched in the
593 phylogeny obtained from mitochondrial genomes (Supplementary Figs. S5 and S6). This
594 helps to explain why most of the previous molecular studies recovered a non-monophyletic
595 *Arctocephalus*, as mtDNA constituted most or all the sequence data used in these studies
596 (e.g., Árnason et al. 2006; Higdon et al. 2007; Wolf et al. 2007; Yonezawa et al. 2009;
597 Churchill et al. 2014; Berta et al. 2018). The position of *A. forsteri* as sister species of *A.*
598 *australis* in our mtDNA tree instead of *A. galapagoensis*, as in our nuclear genome species
599 tree, is also observed in other mtDNA phylogenies (e.g., Wynen et al. 2001; Yonezawa et al.
600 2009). However, studies with mtDNA sequences from multiple individuals from *A. forsteri*
601 and *A. australis* found several lineages in each species that are intermixed (e.g., Yonezawa et
602 al. 2009). This complex picture, in particular the intermixing of lineages, could be explained
603 by ILS since the grouping of *A. australis* and *A. forsteri* occurred in ~0.8% of the simulated
604 trees. However, introgression could also have played a role in the history of this group, as the
605 QuIBL analysis and the f_4-statistics (Fig. 3 and Supplementary Fig. S11) indicated significant
606 admixture between *A. australis* and *A. forsteri* (see below). Intermixing of individuals of *A.*
607 *australis* and *A. galapagoensis* has likewise been reported for mtDNA (Wolf et al. 2007),
608 further emphasizing that the *A. forsteri/australis/galapagoensis* clade warrants further study.

Divergence Times and Biogeographical Inferences

Our results agree with most previous divergence time estimates and fossil dating that supported a North Pacific origin for Otariidae and the split from Odobenidae at ~19 Ma, in the lower Miocene (Fig. 1 and Supplementary Fig. S7 - Demeré et al. 2003; Árnason et al. 2006; Yonezawa et al. 2009; Nyakatura and Bininda-Emonds 2012; Churchill et al. 2014; Berta et al. 2018), when early Odobenidae and Otariidae co-occurred (Boessenecker and Churchill 2015). The divergence of *Callorhinus* at ~9 Ma is also similar to most previous estimates (e.g., Yonezawa et al. 2009; Nyakatura and Bininda-Emonds 2012), although Berta et al. (2018) suggested a much older divergence at ~16 Ma. A comparison of our results with previous divergence times (Yonezawa et al. 2009; Nyakatura and Bininda-Emonds 2012; Berta et al. 2018) is not straightforward given the differences in topologies. Some significant points, however, can be made. First, no previous study detected the explosive radiation at the beginning of the diversification of the southern clade around the Pliocene-Pleistocene boundary. Second, our estimates of divergence between the northern (*C. ursinus*, *Zalophus* spp. and *E. jubatus*) and the southern clades (*O. flavescens*, *P. hookeri*, and *Arctocephalus* spp.) at ~5.3 Ma, and the initial diversification within the northern (~0.25 Ma) and the southern (3-2.5 Ma) clades are younger than most previous estimates (Yonezawa et al. 2009; Nyakatura and Bininda-Emonds 2014; Churchill et al. 2014; Berta et al. 2018). As an extreme example, Berta et al. (2018) estimated the divergence between *Otaria, Phocarctos,* and *Arctocephalus* at >6 Ma. On the other hand, Berta et al. (2018) estimated that the diversifications within *Arctocephalus* (except for the *A. pusillus* + *A. tropicalis* clade) are very recent, <1 Ma. It should be noted that, although we detected possible evidence for three introgression events with only a moderate extent (~10% of genomic introgression, Fig. 3 and below), we may have still underestimated some divergence times since the methods used here did not consider introgression. This may be the case for the very recent speciation times

634 between the three species of the northern clade that could be underestimated due to past
635 introgression events (Fig. 3).

636 Our phylogenomic results broadly agree with a scenario of a relatively recent trans-
637 equatorial dispersal towards the Southern Hemisphere, likely along the Pacific coast of South
638 America (see Yonezawa et al. 2009; Churchill et al. 2014, Berta et al. 2018). For a better
639 understanding of this biogeographical history, we used data such as the age and phylogenetic
640 position of fossils. In the Southern Hemisphere, most of the otariid fossils date back to the
641 Pleistocene, with *Hydrarctos* known from sediments of the end of the Pliocene. *Hydrarctos*
642 (Muizon 1978; Muizon and DeVries 1985; Avery and Klein 2011) is the oldest known otariid
643 fossil from South America and comes from the Pisco Formation of Peru. However, its
644 phylogenetic position is uncertain. It has been more consistently placed within the southern
645 clade due to its morphological similarity with *Arctocephalus* (Muizon 1978), but was also
646 positioned outside the southern clade as the sister taxon to all extant otariids (Churchill et al.
647 2014; Berta et al. 2018). Our divergence time estimates do not support the position of
648 *Hydrarctos* inside the southern clade since the diversification of the latter group started at ~3
649 Mya, and the youngest date of the fossil is ~3.9 Ma (it may be as old as ~6.6 Ma, see Muizon
650 1978; Muizon and DeVries 1985; Churchill et al. 2014). Therefore, *Hydrarctos* is likely a
651 sister clade to the southern clade or, assuming the oldest dates, may represent an independent
652 (and extinct) trans-equatorial dispersal towards the west coast of South America that
653 preceded the one that gave rise to the extant southern clade. *Arctocephalus* sp. nov., a fossil
654 that belongs to the Varswater Formation of South Africa, was dated between ~2.7-5 Ma
655 (Avery and Klein 2011), and we used its most recent date as the minimum age for
656 *Arctocephalus* in our StarBEAST2 calibrated species tree. Our point estimate in the origin of
657 *Arctocephalus* was ~2.8 Ma (95% CI ranging from 2.4 to 3.3 Ma, Fig. 1b), close to the
658 minimum limit. The divergence times of the species tree reestimated using only the calibrated
659 point at the root (20 Ma) with BP&P (Supplementary Fig. S7b) resulted in very similar

660 values, therefore supporting our estimates of diversification of the southern clade dates
661 between ~3 Mya and 2.5 Ma. However, the occurrence of *Arctocephalus* in South Africa at
662 this time means that it had already been established in South America before its eastern
663 dispersal to Africa.

664 Based on these results, dispersal to the Southern Hemisphere could have occurred
665 anytime between ~5 Ma, the split of the southern clade from the northern *Zalophus* group,
666 and ~3 Ma, the beginning of the explosive radiation within the southern clade. However, if
667 *Hydrarctos* is considered a member of the southern clade with a minimum age of ~4 Ma, the
668 southern dispersal could have occurred more than 1 myr before the burst of diversification of
669 the extant species. At the moment, it is not practical to speculate as to the specific moment of
670 the trans-equatorial dispersal within this large interval (between ~3 and 5 Ma). There are,
671 however, environmental conditions within this timeframe that may have facilitated trans-
672 equatorial dispersal such as lower sea temperatures in the equatorial zone (Churchill et al.
673 2014) and its concomitant higher ocean primary productivity. The period between the early
674 Pliocene (~4 Ma) and the mid-Pliocene (~3.5 Ma) was characterized by warm temperatures
675 (Fig. 1c, Fedorov et al. 2013) and low-productivity waters that likely impeded the trans-
676 hemispheric dispersal at that time (O'Dea et al. 2012; Fedorov et al. 2013; Churchill et al.
677 2014). A trans-hemispheric dispersal more recent than estimated in previous studies (>5Ma,
678 e.g., Yonezawa et al. 2009), and closer to the time of the southern clade diversification (~3
679 Ma), better explains the absence of otariids in the North Atlantic waters, since the total
680 closure of the Central American Seaway finished ~3 Ma (O'Dea et al. 2012).

681 Conversely, the rapid diversification of the southern clade over the Southern
682 Hemisphere, occurring during a relatively short time interval (between ~3.0-2.5 Ma), may be
683 more firmly linked to major climatic events. Around 3 Ma, a sharp global cooling started
684 (Fig. 1c), associated with the beginning of the Northern Hemisphere Glaciation (Fedorov et
685 al. 2013; Marlow et al. 2000). The environmental changes caused by the concomitant global

cooling during the Plio-Pleistocene transition and the total closure of the Panama Isthmus would have provided a suitable niche for otariids, driven by the increase of primary productivity in the Southern Pacific Ocean (O'Dea et al. 2012; Churchill et al. 2014). These changes may have opened the way for long-distance dispersal events within the Southern Hemisphere, with the establishment of new colonies and local adaptation to new niches, facilitating rapid speciation.

Genealogical Discordances, ILS and Introgression

We found a high degree of topological discordance between the trees estimated from GFs along genomes (including the single locus mtDNA), with many topologies appearing in only one GF, even in the GFs of 200 kb (Table 2, Supplementary Fig. S8). These results explain the high degree of discordances among the phylogenies estimated by all previous studies and why it has been challenging to find a robust classification for the Otariidae based on a few genes. This high GF tree discordance could not be attributed to a lack of information in the GFs in general since most internal nodes, both older and recent, had high support values (e.g., sCF values in Supplementary Figs. S10). Most of the discordance was concentrated in the four nodes that gave rise to the six main lineages in the southern clade (Fig. 2 and Supplementary Fig. S10) and their extremely short internal branches. The explosive radiation (i.e., fast successive speciation events) at the origin of the southern clade was accompanied by short internal branches increasing the occurrence of ILS (see the small gCF values at theses nodes in Fig. 2) (Suh et al. 2015).

Topological discordance between genomic regions is not unusual and is being observed with increasing frequency in recent phylogenomic studies (e.g., Martin et al. 2013; Li et al. 2016; Pease et al. 2016; Árnason et al., 2018; Sun et al. 2020). The sources of topological discordances are mainly attributed to ILS, as suggested above, and hybridization (Bravo et al. 2019). Recent genomic studies have shown that introgression, mainly inferred with *D*-

712 statistics or related statistics (e.g., ABBA-BABA, *f3*, and *f4*), is widespread in the history of
713 several groups (e.g., Pease et al. 2016; Figueiró et al. 2017; Masello et al. 2019). Here, we
714 suggest that the several rapid successive events of speciation violated the assumptions of the
715 bifurcating species tree and led to substantially false-positive signals of introgression in *f4*
716 analysis, since the extremely short internal nodes do not allow this method to distinguish the
717 true tree from alternative topologies (Durand et al. 2011; Eriksson and Manica 2012;
718 Malinsky et al. 2018). In similar cases, we suggest replacing *f4*-statistics with methods that
719 seem more robust to such artifacts, such as the recently developed QuIBL approach (Edelman
720 et al. 2019). Instead, for a limited number of cases, prominent in the genus *Arctocephalus*,
721 introgression seems to have contributed to the incongruencies. Considering present-day lack
722 of firm reproductive barriers between several *Arctocephalus* species (Churchill et al. 2014),
723 introgression during cladogenesis or shortly thereafter seems indeed plausible.

724 There have been recent implementations in the phylogenetic algorithms to infer
725 divergence times that included hybridization in the multispecies coalescent models to
726 estimate species networks (Zhang et al. 2017; Wen et al. 2018; Wen and Nakhleh 2018; Jones
727 2019). We have tried to recover a species network using four of these methods: the
728 SpeciesNetwork (Zhang et al. 2018) and DENIM (Jones 2019), both implemented in
729 StarBEAST2, and the MCMC_GT and MCMC_SEQ from PhyloNet (Wen et al. 2018). For
730 these analyses, we used 100 GFs of 1 kb and 5 kb selected among those with more variation
731 from the 300 GFs of 50 kb used in the StarBEAST2 analyses (Fig. 1b and Supplementary
732 Fig. S7a). Unfortunately, either the Bayesian estimations did not stabilize even after long runs
733 (>1 billion steps, DENIM), or we recovered several topologies that differed markedly from
734 all other main topologies recovered with other methods (SpeciesNetwork and PhyloNet).
735 Similar inconsistencies have also been found in other studies (e.g., Chen et al. 2019) and
736 could be related to the high complexity of the models with a higher number of taxa (since
737 these methods are mostly recommended for use with less than six taxa). The virtual polytomy

738 between six lineages and the consequent high levels of ILS in our dataset may also have
739 contributed to the non-stabilization of the analyses.

740 The relationships within the clade comprising *A. australis*, *A. galapagoensis*, and *A.*
741 *forsteri* seem to reflect a complex scenario since we found evidence for both introgression
742 and ILS between these species. Furthermore, previous studies based on mtDNA have found
743 the absence of reciprocal monophyly among species (Wynen et al. 2001; Wolf et al. 2007;
744 Yonezawa et al. 2009) and the possible existence of at least one cryptic species (King 1954;
745 Repenning et al. 1971; Wynen et al. 2001; Oliveira et al. 2008; Yonezawa et al. 2009;
746 Oliveira and Brownell 2014). Therefore, this clade needs a more in-depth study, analyzing
747 samples from several populations.

748 CONCLUSIONS

749 1. We used entire genome sequencing for 14 (missing *Neophoca cinerea*) of the extant
750 15 species of Otariidae to determine the phylogeny of this family and its bearing on its
751 taxonomy and biogeographical history. Despite extreme topological discordance among GF
752 trees, we found a fully supported species tree that agrees with the few well-accepted
753 relationships found in previous studies.

754 2. Overall, the substantial degree of genealogical discordance was mostly accounted for
755 by incomplete lineage sorting of ancestral genetic variation, though with a contribution of
756 introgression in some clades.

757 3. A relatively recent trans-equatorial dispersal 3 to 2.5 Ma at the base of the southern
758 clade rapidly diversified into six major lineages. *Otaria* was the first to diverge, followed by
759 *Phocarctos* and then four lineages within *Arctocephalus*. This dispersal most likely occurred
760 along the Pacific coast.

4. We found *Zalophus* and *Eumetopias*, from the northern clade, to be paraphyletic, with California sea lions (*Z. californianus*) more closely related to Steller sea lions (*Eumetopias jubatus*) than to Galapagos sea lions (*Z. wollebaeki*). However, the internal branch separating *Z. wollebaeki* from the other two species is very short, their divergence times are very recent, and we detected a signal of introgression between these two groups. It is necessary to conduct a more in-depth study of this clade, with genomic information from many individuals throughout the species' distributions.

5. Quasi-simultaneous speciation within the southern clade led to extensive incomplete lineage sorting throughout the genomes, resulting in a high level of genealogical discordance, which explains the incongruence among and within prior phylogenetic studies of the family.

6. We suggest the use of recently developed methods of QuIBL when rapid successive events of speciation are detected to quantify events of genomic introgression. In similar cases, *f4*-statistics can violate the assumptions of the bifurcating species tree, leading to substantially false-positive signals of introgression.

7. Resolving a long-standing controversy, we found that the genus *Arctocephalus* is monophyletic, which makes the genus *Arctophoca* a junior synonym of *Arctocephalus*.

SUPPLEMENTARY MATERIAL

- Raw sequencing data is available at NCBI BioProject PRJNA576431

- Data available from the Dryad Digital Repository: doi:10.5061/dryad.pzgmsbchw

FUNDING

This work was mainly supported by grants from CNPq and FAPERGS (PRONEX 12/2014) governmental agencies in Brazil to S.L.B, a US Navy NICOP 2015 granted to Eduardo Eizirik and S.L.B., CNPq Research Productivity Fellowships (to S.L.B: 310472/2017-2, and to L.R.O.: 308650/2014-0 and 310621/2017-8). Funding was further provided by the Swedish Research Council (FORMAS) and LMU Munich to J.W, Coordenação de Aperfeiçoamento de Pessoal de Nivel Superior (CAPES) (Brazil**)** – Finance Code 001 Ph.D. scholarship, Society for Marine Mammalogy Small Grants-in-aid of Research 2016, and CNPq INCT-EECBio process number 380752/2020-4 to F.L.

ACKNOWLEDGMENTS

We are very thankful for the support of all people and institutions that contributed to this manuscript. We are also very grateful for the support of GEMARS, NOAA-SWFSC and Kelly Robertson which contributed with samples; Laboratório de Biologia Genômica e Molecular-PUCRS staff and students for support, general suggestions, and discussions; Jochen B. W. Wolf Group and Ludwig-Maximilians-Universität München which kindly hosted F.L. in his sandwich Ph.D.; two anonymous reviewers, and the associate editor and editor-in-chief for their helpful comment; and Nathaly Miranda who reviewed many versions of this manuscript.

CONFLICT OF INTEREST

The authors declare no conflict of interest.

REFERENCES

Árnason U., Lammers F., Kumar V., Nilsson M.A., Janke A. 2018. Whole-genome sequencing of the blue whale and other rorqual finds signatures for introgressive gene flow. Sci. Adv. 4:eaap9873

Árnason U., Gullberg A., Janke A., Kullberg M., Lehman N., Petrov E.A., Väinölä R. 2006. Pinniped phylogeny and a new hypothesis for their origin and dispersal. Mol. Phylogenet. Evol. 41:345-354

Arnold B., Corbett-Detig R.B., Hartl D., Bomblies K. 2013. RADseq underestimates diversity and introduces genealogical biases due to nonrandom haplotype sampling. Mol. Ecol. 22:3179-3190.

Andrews S. 2010. FastQC: a quality control tool for high throughput sequence data. Available online at http://www.bioinformatics.babraham.ac.uk/projects/fastqc

Aurioles-Gamboa D. 2015. *Arctocephalus philippii*. The IUCN Red List of Threatened Species 2015: e.T2059A61953525

Avery G., Klein R.G. 2011. Review of fossil phocid and otariid seals from the southern and western coasts of South Africa. T. Roy. Soc. S. Afr. 66:14-24

Benton M.J., Ayala F.J. 2003. Dating the Tree of Life. Science 300:1698-1700

Berta A., Churchill M. 2012. Pinniped taxonomy: Review of currently recognized species and subspecies, and evidence used for their description. Mamm. Rev. 42:207-234

Berta A., Churchill M., Boessenecker R.W. 2018. The origin and evolutionary biology of pinnipeds: seals, sea lions and walruses. Annu. Rev. Earth. Planet. Sci. 46:203-228

Berta A., Deméré T.A. 1986. *Callorhinus gilmorei* n. sp., (Carnivora: Otariidae) from the San Diego Formation (Blancan) and its implications for otariid phylogeny. Trans. San. Diego. Soc. Nat. Hist. 21:111-116

831 Boessenecker R.W. 2011. New Records of the fur seal *Callorhinus ursinus* (Carnivora: Otariidae)
832 from the Plio-Pleistocene Rio Dell formation of the Northern California and comments on otariid
833 dental evolution. J. Vert. Paleontol. 31:454-467

834 Boessenecker R.W., Churchill M. 2015. The oldest known fur seal. Biol. Lett. 11:20140835

835 Borowiec M.L. 2016. AMAS: a fast tool for alignment manipulation and computing of summary
836 statistics. PeerJ 4:e1660

837 Bouckaert R., Heled J., Kühnert D., Vaughan T., Wu C. H., Xie D., Suchard M. A., Rambaut A.,
838 Drummond A. J. 2014. BEAST 2: a software platform for Bayesian evolutionary analysis. PLoS
839 Comput. Biol. 10:e1003537

840 Bravo G.A., Antonelli A., Bacon C.D., Bartoszek K., Blom M.P.K., Huynh S., Jones G., Knowles
841 L.L., Lamichhaney S., Marcussen T., Morlon H., Nakhleh L.K., Oxelman B., Pfeil B., Schliep
842 A., Wahlberg N., Werneck F.P., Wiedenhoeft J., Willows-Munro S., Edwards S.V. 2019.
843 Embracing heterogeneity: coalescing the Tree of Life and the future of phylogenomics. PeerJ
844 7:e6399

845 Brunner S. 2004. Fur seals and sea lions (Otariidae): Identification of species and taxonomic review.
846 Syst. Biodivers. 1:339-439

847 Capella-Gutierrez S., Silla-Martinez J.M., Gabaldon T. 2009. trimAl: a tool for automated alignment
848 trimming in large-scale phylogenetic analyzes. Bioinformatics 25:1972-1973

849 Chakrabarty P., Faircloth B.C., Alda F., Ludt W.B., McMahan C.D., Near T.J., Dornburg A., Albert
850 J.S., Arroyave J., Stiassny M.L.J., Sorenson L., Alfaro M.E. 2017. Phylogenomic systematics of
851 Ostariophysan fishes: ultraconserved elements support the surprising non-monophyly of
852 Characiformes. Syst. Biol. 66:881-895

853 Chang C.C., Chow C.C., Tellier L.C.A.M., Vattikuti S., Purcell S.M., Lee J.J. 2015. Second-
854 generation PLINK: rising to the challenge of larger and richer data sets. GigaScience 4

855 Chen L., Qiu Q., Jiang Y., Wang K., Lin Z., Li Z., Bibi F., Yang Y., Wang J., Nie W., Su W., Liu G.,
856 Li Q., Fu W., Pan X., Liu C., Yang J., Zhang C., Yin Y., Wang Y., Zhao Y., Zhang C., Wang
857 Z., Qin Y., Liu W., Wang B., Ren Y., Zhang R., Zeng Y., Fonseca R.R., Wei B., Li R., Wan W.,
858 Zhao R., Zhu W., Wang Y., Shengchang D., Gao Y., Zhang Y.E., Chen C., Hvilson C., Epps
859 C.W., Chemnick L.G., Dong Y., Mirarab S., Siegismund H.R., Ryder O., Gilbert M.T., Lewin
860 H.A., Zhang G., Heller R., Wang W. 2019. Large-scale ruminant genome sequencing provides
861 insights into their evolution and distinct traits. Science. 364: 10.1126/science.aav6202

862 Churchill M., Boessenecker R.W., Clementz M.T. 2014. Colonization of the southern hemisphere by
863 fur seals and sea lions (Carnivora: Otariidae) revealed by combined evidence phylogenetic and
864 Bayesian biogeographical analysis. Zool. J. Linn. So.c 172:200-225

865 Committee on Taxonomy of Marine Mammals. 2020. List of marine mammals species and
866 subspecies. Available fromhttps://www.marinemammalscience.org/species-information/list-
867 marine-mammal-species-subspecies

868 Darriba D., Posada D., Kozlov A. M., Stamatakis A., Morel B., Flouri T. 2019. ModelTest-NG: A
869 new scalable tool for the selection of DNA and Protein Evolutionary Models. Mol. Biol. Evol.
870 msz189, https://doi.org/10.1093/molbev/msz189

871 Dasmahapatra K.K., Hoffman J.I., Amos W. 2009. Pinniped phylogenetic relationships inferred using
872 AFLP markers. Heredity. 103:168-177

873 Degnan J.H. 2018. Modeling hybridization under network multispecies coalescent. Syst. Biol. 5:786-
874 799

875 Deméré T.A., Berta A., Adam P.J. 2003. Pinnipedimorph evolutionary biogeography. B. Am. Mus.
876 Nat. His. 279:32-76

877 Drummond A.J., Bouckaert R.R. 2015. Bayesian evolutionary analysis with BEAST. Cambridge
878 University Press. Cambridge 244 pp.

879 Durand E.Y., Patterson N., Reich D., Slatkin M. 2011. Testing for ancient admixture between closely
880 related populations. Mol. Biol. Evol. 28:2239–2252

881 Edelman N.B., Frandsen P.B., Miyagi M., Clavijo B., Davey J., Dikow R.B., García-Accinelli G.,
882 Van Belleghem S.M., Patterson N., Neafsey D.E., Challis R., Kumar S., Moreira G.R.P., Salazar
883 C., Chouteau M., Counterman B.A., Papa R., Blaxter M., Reed R.D., Dasmahapatra K.K.,
884 Kronforst M., Joron M., Jiggins C.D., McMillan W.O., Di Palma F., Blumberg A.J., Wakeley J.,
885 Jaffe J. 2019. Genomic architecture and introgression shape a butterfly radiation. Science.
886 366:594-599

887 Elworth R.A.L., Ogilvie H.A., Zhu J., Nakhleh L. 2019. Advances in computational methods for
888 phylogenetic networks in the presence of hybridization. In Warnow T (ed.) Bioinformatics and
889 Phylogenetics: Seminal Contributions of Bernard Moret. Springer International Publishing

890 Eriksson A., Manica A. 2012. Effect of ancient population structure on the degree of polymorphism
891 shared between modern human populations and ancient hominins. Proc. Natl. Acad. Sci. USA
892 109:13956-13960

893 Esselstyn J.A., Oliveros C.H., Swanson M.T., Faircloth B.C. 2017. Investigating difficult nodes in
894 the placental mammal tree with expanded taxon sampling and thousands of ultraconserved
895 elements. Genome Biol. Evol. 9:2308-2321

896 Faircloth B.C., Sorenson L., Santini F., Alfaro M.E. 2013. A phylogenomic perspective on the
897 radiation of ray-finned fishes based upon target sequencing of ultraconserved elements (UCEs).
898 PLoS One 8:e65923

899 Fedorov A.V., Brierly C.M., Lawrence K.T., Liu Z., Dekens P.S., Ravelo A.C. 2013. Patterns and
900 mechanisms of early Pliocene warmth. Nature 496:43-49

901 Felsestein J. 1989. PHYLIP - Phylogeny Inference Package (Version 3.2). Cladistics 5:164-166

902 Figueiró H.V., Li G., Trindade F., Assis J., Pais F., Fernandes G., Santos S.H., Hughes G.M.,
903 Komissarov A., Antunes A., Trinca C.S., Rodrigues M.R., Linderoth T., Bi K., Silveira L.,

Azevedo F.C.C., Kantek D., Ramalho E., Brassaloti R.A., Villela P.M.S., Nunes A.L.V., Teixeira R.H.F., Morato R.G., Loska D., Saragüeta P., Gabaldón T., Teeling E.C., O'Brien S.J.O., Nielsen R., Coutinho L.L., Oliveira G., Murphy W.J., Eizirik E. 2017. Genome-wide signatures of complex introgression and adaptive evolution in the big cats. Sci. Adv. 7:e1700299

Flouri T., Jiao X., Rannala B., Yang Z. 2018. Species Tree Inference with BPP using Genomic Sequences and the Multispecies Coalescent. Mol. Biol. Evol. 35:2585-2593

Foote A.D., Liu Y., Thomas G.W., Vinař T., Alföldi J., Deng J., Dugan S., van Elk C.E., Hynter M.E., Joshi V., Khan Z., Kovar C., Lee S.L., Linbald-Toh K., Mancia A., Nielsen R., Qin X., Qu J., Raney B.J., Vijay N., Wolf J.B.W., Hahn M.W., Muzny D.M., Worley K.C., Gilbert M.T., Gibbs R.A. 2015. Convergent Evolution of the genomes of marine mammals. Nat. Genet. 47:272-275

Gautier M., Gharbi K., Cezard T., Foucaud J., Kerdelhué C., Pudlo P., Cornuet J.M., Estoup A. 2013. The effect of RAD allele dropout on the estimation of genetic variation within and between populations. Mol. Ecol. 22:3165–3178

Griffiths R.C., Marjoram P. 1997. An ancestral recombination graph. Institute for Mathematics and Its Applications. 87:257

Harris A.M., DeGiorgio M. 2012. Admixture and ancestry inference from ancient and modern samples through measures of population genetic drift. Hum. Biol.114

Higdon J.W., Bininda-Emonds O.R.P., Beck R.M.D., Ferguson S.H. 2007. Phylogeny and divergence of the pinnipeds (Carnivora: Mammalia) assessed using a multigene dataset. BMC Evol. Biol. 7:216

Hoban S.M., Gaggiotti O.E., Bertorelle G. 2013. The number of markers and samples needed for detecting bottlenecks under realistic scenarios, with and without recovery: a simulation-based study. Mol. Ecol. 22:3444-3450

928 Hudson R.R. 1983. Properties of a neutral allele model with intragenic recombination. Theor. Popul.
929 Biol. 23:183-201

930 Hudson R.R., Coyne J.A., Huelsenbeck J.2002. Mathematical consequences of the genealogical
931 species concept. Evolution 56:1557-1565Mol. Ecol. 22:3444-3450

932 Humble E., Martinez-Barrio A., Forcada J., Trathan P.N., Thorne M.A.S., Hoffmann M., Wolf
933 J.B.W., Hoffman J.I. 2016. A draft fur seal genome provides insights into factors affecting SNP
934 validation and how to mitigate them. Mol. Ecol. Res. 16(4):909-921

935 Humble E., Dasmahapatra K.K., Martinez-Barrio A., Gregório I., Forcada J., Polikeit A.C.,
936 Goldsworthy S.D., Goebel M.E., Kalinowski J., Wolf J.B.W., Hoffman J.I. 2018. RAD
937 Sequencing and a Hybrid Antarctic Fur Seal Genome Assembly Reveal Rapidly Decaying
938 Linkage Disequilibrium, Global Population Structure and Evidence for Inbreeding. G3
939 (Bethesda) 31:2709-2722

940 Huson D.H., Scornavacca C. 2012. Dendroscope 3: an interactive tool for rooted phylogenetic trees
941 and networks. Syst Biol 6:1061-1067

942 IUCN Red List of Threatened Species. Version 2017-3 (IUCN, 2017). https://www.iucnredlist.org.
943 Downloaded on 09 July 2020

944 IUCN Red List of Threatened Species. Version 2020-2 (IUCN, 2020). https://www.iucnredlist.org.
945 Downloaded on 09 July 2020

946 Jones G.R. 2019. Divergence estimation in the presence of incomplete lineage sorting and migration.
947 Syst. Biol. 68:19-31

948 Junier T., Zdobnov E.M. 2010. The newick utilities: high-throughput phylogenetic tree processing
949 using unix shell. Bioinformatics 26:1669-1670

950 King J. 1954. The otariid seals of the Pacific coast of America. Bull. Brit. Mus. Zool. 2:311-337

951 Kozlov A. M., Darriba D., Flouri T., Mreol B., Stamatakis A. 2019. RAxML-NG: a fast, scalable
952 andu ser-friendly tool for maximum likelihood phylogenetic information. Bioinformatics.
953 35:4453-4455

954 Korneliussen T.S., Albrechtsen A., Nielsen R. 2014. ANGSD: analysis of Next Generation
955 Sequencing Data. BMC Bioinformatics 15:356

956 Kumar S., Subramanian S. 2001. Mutation rates in mammalian genomes. Proc. Natl. Acad. Sci. U. S.
957 A. 22:803-808

958 Lam H.M., Ratmann O., Boni M.F. 2018. Improved algorithmic complexity for 3seq recombination
959 detection algorithm. Mol. Biol. Evol. 35:247-251

960 Lancaster M.L., Gemmell N.J., Negro S., Goldsworthy S., Sunnucks P. 2006. Ménage à trois on
961 Macquarie Island: hybridization among three species of fur seal (*Arctocephalus* spp.) following
962 historical population extinction. Mol. Ecol. 15:3681-3692

963 Leaché A.D., Harris R.B., Rannala B., Yang Z. 2014. The influence of gene flow on species tree
964 estimation: a simulation study. Syst. Biol. 63:17-30

965 Leppälä K., Nielsen S., Mailund T. 2017. admixturegraph: an R package for admixture graph
966 manipulation and fitting. Bioinformatics 33:1738-1740

967 Li H., Durbin R. 2009. Fast and accurate short read alignment with Burrows-Wheeler Transform.
968 Bioinformatics 25:1754-60

969 Li G., Davis B.W., Eizirik E., Murphy W.J. 2016. Phylogenomic evidence for ancient hybridization
970 in the genomes of living cats (Felidae). Genome Res. 26:1-11

971 Liu L., Yu L. 2010. Phybase: an R package for species tree analysis. Bioinformatics 26:962-963

972 Maddison W.P., Knowles L.L. 2006. Inferring phylogeny despite incomplete lineage sorting. Syst.
973 Biol. 55:21-30

974 Malinsky M. 2019. Dsuite - fast D-statistics and related admixture evidence from VCF files. doi:
975 doi.org/10.1101/634477

976 Malinsky M., Svardal H., Tyers A.M., Miska E.A., Genner M.J., Turner G.F., Durbin R. 2018.
977 Whole-genome sequences of Malawi cichlids reveal multiple radiations interconnected by gene
978 flow. Nat. Ecol. Evol. 2:1940-1955

979 Marlow J.R., Lange C.B., Wefer G., Rosell-Melé A. 2000. Upwelling intensification as part of the
980 Pliocene-Pleistocene climate transition. Science 22:2288-2291

981 Martin S.H., Dasmahapatra K.K., Nadeau N.J., Salazar C., Walters J.R., Fraser S., Blaxter M., Manica
982 A., Mallet J., Jiggins C.D. 2013. Genome-wide evidence for speciation with gene flow in
983 *Heliconius* butterflies. Genome Res. 23:1817-1828

984 Masello J.F., Quillfeldt P., Sandoval-Castellanos E., Alderman R., Calderón L., Cherel Y., Cole T.L.,
985 Cuthbert R.J., Marin M., Massaro M., Navarro J., Phillips R.A., Shepherd L.D., Suazo C.g.,
986 Weimerskirch H, Moodley Y. Additive traits lead to feeding advantage and reproductive
987 isolation, promoting homoploid hybrid speciation. Mol. Biol. Evol. 36:1671-1685

988 McCormack J.E., Faircloth B.C. 2013. Next-generation phylogenetics takes root. Mol. Ecol. 22:19-
989 21

990 McKenna A., Hanna M., Banks E., Sivachenko A., Cibulskis K., Kernytsky A., Garimella K.,
991 Altshuler D., Gabriel S., Daly M., dePristo M.A. 2010. The Genome Analysis Toolkit: a
992 MapReference framework for analyzing next-generation DNA sequencing data. Genome Res.
993 20:297-303

994 Minh B. Q., Hahn M. W., Lanfear R. 2018. New method to calculate concordance factors for
995 phylogenomic datasets. doi.org/10.1101/487801

996 Mugal C.F., Kutschera V.E., Botero-Castro F., Wolf J.B.W., Kaj I. 2020. Polymorphism Data Assist
997 Estimation of the Nonsynonymous over Synonymous Fixation Rate Ratio ω for Closely Related
998 Species. Mol. Biol. Evol. 37:260-279

999 Muizon C. 1978. *Arctocephalus* (*Hydrarctos*) lomasiensis, subgen. nov. et. nov sp., un unouvel
1000 Otariidae du Mio-Pliocene de Sacaco. B. I'Inst. Franc. d'Etu. And. 7:169189

1001 Muizon C., DeVries T.J. 1985. Geology and paleontology of late cenozoic marine deposits in the
1002 Sacaco area (Peru). Geol. Rundsch. 74:547-563

1003 Nabholz B., Glémin S., Galtier N. 2007. Strong variations of mitochondrial mutation rate across
1004 mammals – the longevity hypothesis. Mol. Biol. Evol. 25:120-130

1005 Nakhleh L. 2013. Computational approaches to species phylogeny inference and gene tree
1006 reconciliation. Trends. Ecol. Evol. 28:719-728

1007 Nguyen L. T., Schmidt H. A., von Haeseler A., Minh B. Q. 2015. IQ-TREE: A fast and effective
1008 stochastic algorithm for estimating maximum likelihood phylogenies. Mol. Biol. Evol., 32:268-
1009 274

1010 Nyakatura K., Bininda-Emonds O.R.P. 2012. Updating the evolutionary history of Carnivora
1011 (Mammalia): A new species-level supertree complete with divergence time estimates. BMC Biol.
1012 10:12. doi:10.1186/1741-7007-10-12

1013 O'Dea A., Hoyos N., Rodriguez F., Degracia B., De Gracia C. 2012. History of upwelling in the
1014 Tropical Eastern Pacific and the palaeogeography of the Isthmus of Panama. Palaeograph.
1015 Palaeoclimat. Palaeoecol. 348-349:59-66

1016 Ogilvie H.A., Bouckaert R.R., Drummond A.J. 2017. StarBEAST2 Brings faster species tree
1017 inference and accurate estimates of substitution rates. Mol. Biol. Evol. 34:2101-2114

1018 Oliveira L., Hoffman J.I., Hingst-Zaher E., Majluf P., Muelbert M.MC., Morgante J.S. 2008.
1019 Morphological and genetic evidence for two evolutionarily significant units (ESUs) in the South
1020 American fur seal, Arctocephalus australis. Conserv. Genet. 9:1451-1466.

1021 Oliveira L., Brownell Jr. R.L. 2014. Taxonomic status of two subspecies of South American fur seals:
1022 *Arctocephalus australis australis* vs. *A. a. gracilis*. Mar. Mamm. Sci. 30:1258-1263

1023 Oliver J.C. 2013. Microevolutionary process generates phylogenomic discordance at ancient
1024 divergence. Evolution 5:568-583

1025 Patterson N., Moorjani P., Luo Y., Mallick S., Rohland N., Zhan Y., Genschoreck T., Webster T.,
1026 Reich D.2012. Ancient Admixture in Human History. Genetics 192:1065-1093

1027 Peart C.R., Tusso S., Pophaly S.D., Botero-Castro F., Wu C.C., Aurioles-Gamboa D., Baird A. B.,
1028 Bickham J.W., Forcada J., Galimberti F., Gemmel N. J., Hoffman J.I., Kovacs K.M., Kunnasranta
1029 M., Lydersen C., Nyman T., Oliveira L.R., Orr A.J., Sanvito S., Valtonen M., Shafer A.B.A.,
1030 Wolf J.B.W. 2020. Determinants of genetic variation across eco-evolutionary scales in pinnipeds.
1031 Nat. Ecol. Evol. https://doi.org/10.1038/s41559-020-1215-5

1032 Pease J.B., Haak D.C., Hahn M.W., Moyle L.C. 2016. Phylogenomics reveals three sources of
1033 adaptive variation during rapid radiation. PLoS Biol 14(2):e1002379

1034 Peter B.M. 2016. Admixture, population structure, and *F*-statistics. Genetics 202:1485-1501

1035 Pickrell J.K., Pritchard J.K. 2012. Inference of population splits and mixtures from genome-wide
1036 allele frequency data. PLoS Genet. 8:e1002967

1037 Quinlan A.R., Hall I.M. 2010. BEDTools: a flexible suite of utilities for comparing genomic features.
1038 Bioinformatics 6:841-842

1039 Rambaut A., Drummond A.J. 2007. Tracer v1.7 Available from https://github.com/beast-
1040 dev/tracer/releases/latest

1041 Rambaut A., Drummond A.J. 2010. TreeAnnotator version 1.6.1 Available from
1042 http://beast.bio.ed.ac.uk

1043 Rambaut A. 2017. FigTree v1.4.4. Available from: https://github.com/rambaut/figtree/

1044 Reddy S., Kimball R.T., Pandey A., Hosner P.A., Braun M.J., Hackett S.J., Han K.L., Harshmann J.,
1045 Huddleston C.J., Kingston S., Marks B.D., Miglia K.J., Moore W.S., Sheldon F.H., Witt C.C.,

1046 Yuri T.B., Braun E.L. 2017. Why do phylogenomic data sets yield conflicting trees? Data type
1047 influences the avian Tree of Life more than taxon sampling. Syst. Biol. 66:857-879

1048 Repenning C.A., Peterson R.S., Hubbs C.L. 1971. Contributions to the systematics of the southern
1049 fur seals, with particular reference to the Juan Fernández and Guadalupe species. Antarct. Res.
1050 S. 18:1-34

1051 Rice W.R. 1989. Analyzing tables of statistical tests. Evolution 43:223-225

1052 Rheindt F.E., Fujita M.K., Wilton P.R., Edwards S.V. 2014. Introgression and phenotypic
1053 assimilation in *Zimmerius* flycatchers (Tyrannidae): population genetic and phylogenetic
1054 inferences from genome-wide SNPs. Syst. Biol. 63:134-152

1055 Rokas A., Williams B.L., King N., Carrol S.B. 2003. Genome-scale approaches to resolving
1056 incongruence in molecular phylogenies. Nature 425:798-804

1057 Rosenberg N.A. 2003. The Shapes of Neutral Gene Genealogies in Two Species: Probabilities of
1058 Monophyly, Paraphyly, and Polyphyly in a Coalescent Model. Evolution 57:1465-1477

1059 Schramm Y., Mesnick S.L., Rosa J. de la, Palacios D.M., Lowry M.S., Aurioles-Gamboa D., Snell
1060 H.M., Escorza-Treviño S. 2009. Phylogeography of California and Galápagos sea lions and
1061 population structure within the California sea lion. Mar. Biol. 156:1375-1387

1062 Schubert M., Ermini L., Sarkissian C.D., Jónsson H., Ginolhac A., Schaefer R., Martin M.D.,
1063 Fernández R., Kircher M., McCue M., Willerslev E., Orlando L. 2014. Characterization of
1064 ancient and modern genomes by SNP detection and phylogenomic and metagenomic analysis
1065 using PALEOMIX. Nat. Protoc. 9:1056-1082

1066 Schubert M., Lindgreen S., Orlando L. 2016. AdapterRemoval v2: rapid adapter trimming,
1067 identification, and read merging. BMC Res. Notes 9:88

1068 Sclater P.L. 1897. On the distribution of marine mammals. Proc. Zool. Soc. London, 349–359

1069 Scheffer V.B. 1958. Seals, sea lions and walruses. Stanford: Stanford University Press

1070 Shafer A.B.A., Peart C.R., Tusso S., Maayan I., Brelsford A., Wheat C.W., Wolf J.B.W. 2017.
1071 Bioinformatic processing of RAD-seq data dramatically impacts downstream population genetic
1072 inference. Meth. Ecol. Evol. 8:907-017

1073 Stamatakis A. 2014. RAxML version 8: a tool for phylogenetic analysis and post-analysis of large
1074 phylogenies. Bioinformatics 30:1312-1313

1075 Suh A., Smeds L., Ellegreen H. 2015. The Dynamics of Incomplete Lineage Sorting across the
1076 Ancient Adaptive Radiation of Neoavian Birds. PLoS Biol. 13:e1002224

1077 Sun C., Huang J., Zhao X., Su L., Thomas G.W.C., Zhao M., Zhang X., Jungreis I., Kellis M., Vicario
1078 S., Sharakhov I.V., Bondarenko S.M., Hasselmann M., Kim C.N., Paten B., Penso-Dolfin L.,
1079 Wang L., Chang Y., Gao Q., Ma L., Ma L., Zhang Y., Zhang H., Ruzzante L., Robertson H.M.,
1080 Zhu Y., Liu Y., Yang H., Ding L., Wang Q., Ma D., Xu W., Liang C., Itgen M.W., Mee L., Cao
1081 G., Zhang Z., Sadd B.M., Hahn M., Schaak S., Barribeau S.M., Williams P.H., Waterhouse R.M.,
1082 Mueller R.L. 2020. Genus-wide characterization of bumblebee genomes provides insights into
1083 their evolution and variation in ecological and behavioral traits. Mol. Biol. Evol.
1084 doi.org/10.1093/molbev/msaa240

1085 Wang K., Lenstra J.A., Liu L., Hu Q., Ma T., Qiu Q., Liu J. 2018. Incomplete lineage sorting rather
1086 than hybridization explains the inconsistent phylogeny of the wisent. Comm. Biol. 1:169

1087 Wen D., Nakhleh L. 2018. Coestimating reticulate phylogenies and gene trees from multilocus
1088 sequence data. Syst. Biol. 67:439-457

1089 Wen D., Yu Y., Nakhleh L. 2018. Inferring phylogenetic networks using Phylonet. Syst. Biol. 67:735-
1090 740

1091 Wolf J.B.W., Tautz D., Trillmich F. 2007. Galápagos and Californian sea lions are separate species:
1092 genetic analysis of the genus *Zalophus* and its implications for conservation management. Front.
1093 Zool. 4:1-13

1094 Wolf J.B.W., Harrod C., Brunner S., Salazar S., Trillmich F., Tautz D. 2008. Tracing early stages of
1095 species differentiation: Ecological, morphological and genetic divergence of Galapagos sea lion
1096 populations. BMC Evol. Biol. 8:150

1097 Wynen L.P., Goldsworthy S.D., Insley S.J., Adams M., Bickham J.W., Francis J., Gallo J.P., Hoelzel
1098 A.R., Majluf P., White R.W.G., Slade R. 2001. Phylogenetic relationships within eared seals
1099 (Otariidae: Carnivora): implications for the historical biogeography of the family. Mol.
1100 Phylogenet. Evol. 21:270-284

1101 Yonezawa T., Kohno N., Hasegawa M. 2009. The monophyletic origin of sea lion and fur seals
1102 (Carnivora: Otariidae) in the southern hemisphere. Gene 441:89-99

1103 Zhang C., Ogilvie H.A., Drummond A.J., Stadler T. 2017. Bayesian inference of species networks
1104 from multilocus sequence data. Mol. Biol. Evol. 35:504-517

1105 Zhang C., Rabiee M., Sayyari E., Mirarab S. 2018. ASTRAL-III: polynomial time species tree
1106 reconstruction from partially resolved gene trees. BMC Bioinformatics, 19 (suppl 6):153

1107 Zheng Y., Janke A. 2018. Gene flow analysis method, the D-statistic, is robust in a wide parameter
1108 space. BMC Bioinformatics. 19:10

1109 Ziheng Y. 2015. The BPP program for species tree estimation and species delimitation. Curr. Zool.
1110 61:854-865

1111
1112
1113
1114
1115
1116
1117
1118
1119
1120

Legends

Table 1. Whole genome shotgun sequences produced for this study (in bold) and obtained from GenBank digital repository.

Table 2. The ten most frequent topologies for the southern clade estimated with RAxML in each GF dataset and the absolute frequencies of occurrence in the different sets of windows sizes.

Figure 1. (a) Current distribution of fur seals and sea lions obtained from the IUCN Red List (IUCN 2020). *A. galapagoensis* (Agal) and *Z. wollebaeki* (Zwol) have very similar and small distributions and are represented with the same color and an arrow. *A. philippii* (Aphi) is endemic to the Juan Fernández Island, and its distribution is also represented with an arrow. The symbols represent the four sites of the past temperature data in "c." (b) Time calibrated Bayesian species tree estimated with StarBEAST2 using 300 GFs of 50 kb. Blue bars represent the divergence time 95% confidence interval. The vertical gray bar represents the 95% confidence interval of the period of fast diversification of the southern clade. All nodes have the highest posterior density (HPD) = 1 except for the *Arctocephalus* node (HPD = 0.92), shown as an open circle in the phylogeny. (c) The Sea Surface Temperature (SST) temperature data from four sites in the Tropical and Subtropical Pacific eastern Pacific (Fedorov et al. 2013). The vertical gray bar represents the same time interval depicted in the species tree.

Figure 2. Gene concordance factor (gCF) for the nodes (14-23) that support (red bars) the species tree (bottom right) and the two most common alternative resolutions (gDF1 and gDF2, blue and green bars, respectively). The yellow bars are the relative frequencies of all other alternative resolutions. The nodes showing lower concordance factors (16, 17, 19 and 20) represent the lineages of fast radiation of eared seals in the Southern Hemisphere, with a remarkable number of alternative resolutions. These nodes are represented with an asterisk in the species tree.

Figure 3. QuIBL significant results. The table at the left shows three alternative relationships for each species trio tested (the last of which, in grey type, is the species tree), the number of GF trees that significantly supported that relationship, and the proportion of these trees that could be explained by ILS or by alternative explanations (non-ILS, i.e., introgression or the phylogeny itself). Total non-ILS is the percentage of all GF trees that were introgressed between the pair of species that are not the outgroup (in the species tree this is explained by the phylogeny). To the right is the species tree depicting the introgression events supported.

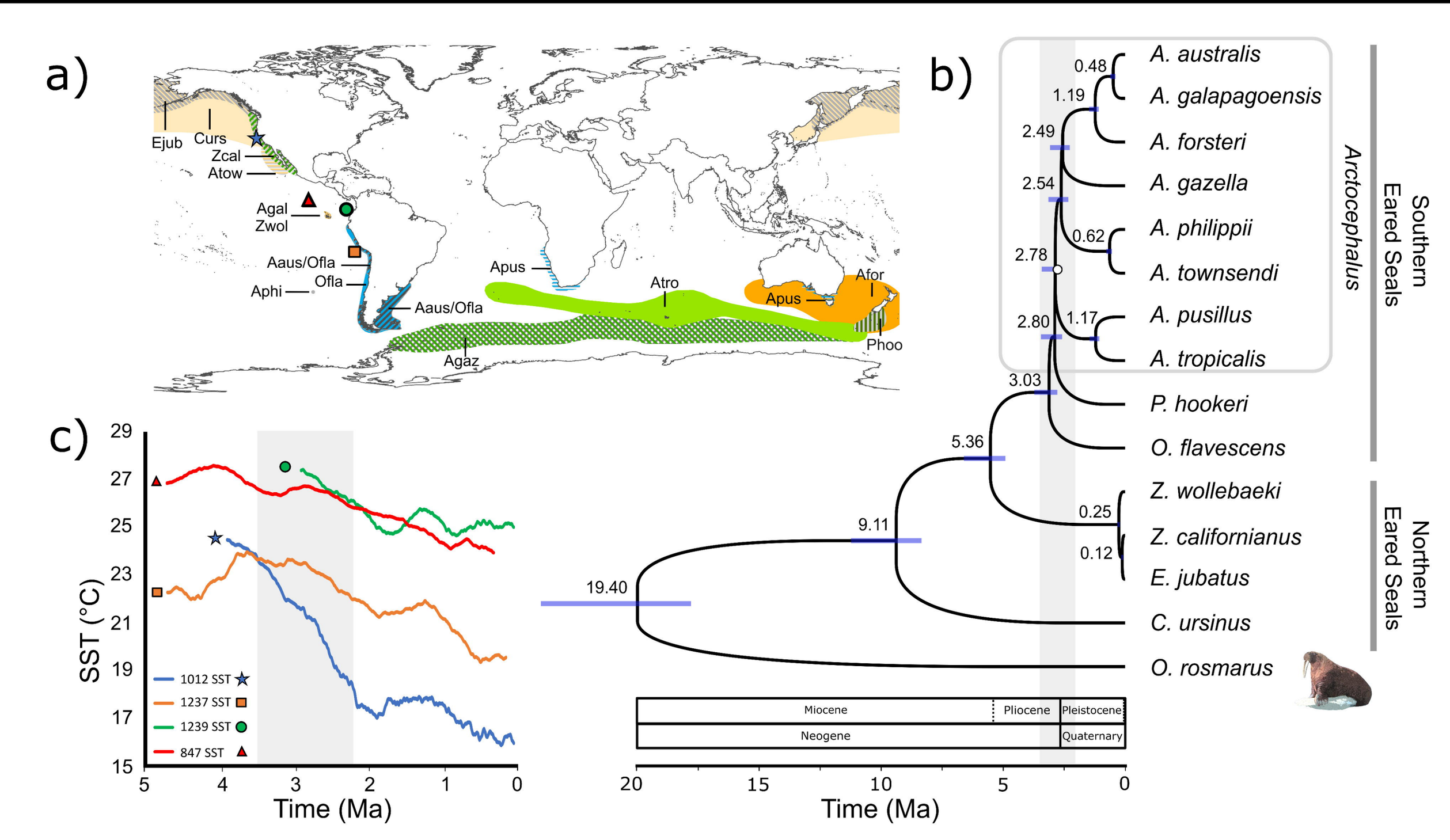
a)
Ejub
Curs
Zcal
Atow
Agal
Zwol
Aaus/Ofla
Ofla
Aphi
Aaus/Ofla
Apus
Atro
Apus
Afor
Phoo
Agaz
b)
A. australis
A. galapagoensis
A. forsteri
A. gazella
A. philippii
A. townsendi
A. pusillus
A. tropicalis
P. hookeri
O. flavescens
Z. wollebaeki
Z. californianus
E. jubatus
C. ursinus
O. rosmarus
0.48
1.19
2.49
2.54
0.62
2.78
1.17
2.80
3.03
5.36
0.25
0.12
9.11
19.40
Arctocephalus
Southern Eared Seals
Northern Eared Seals
Miocene
Pliocene
Pleistocene
Neogene
Quaternary
20
15
10
5
0
Time (Ma)
c)
SST (°C)
29
27
25
23
21
19
17
15
1012 SST
1237 SST
1239 SST
847 SST
5
4
3
2
1
0
Time (Ma)

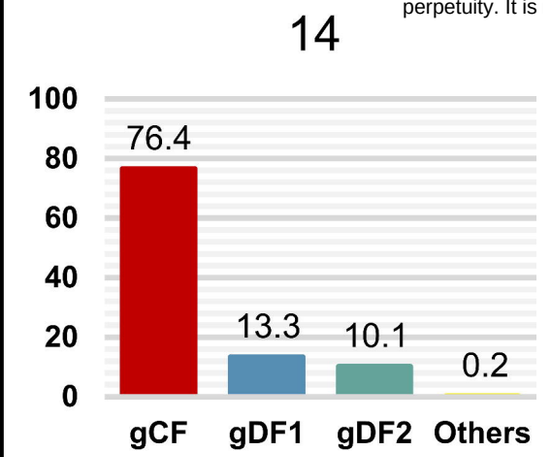

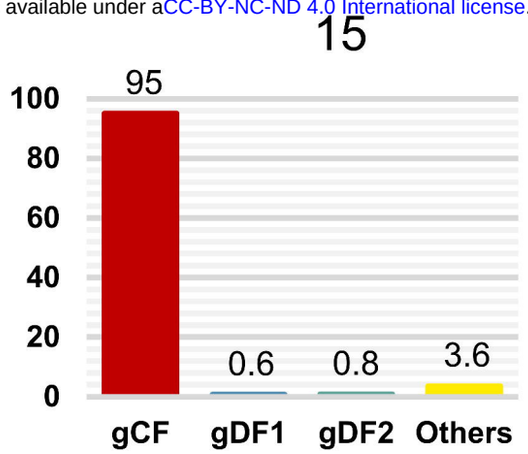

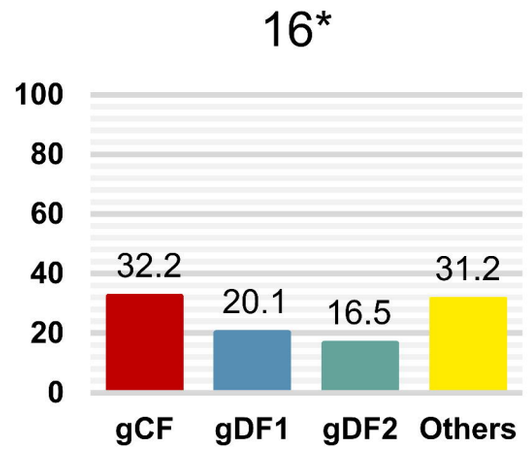

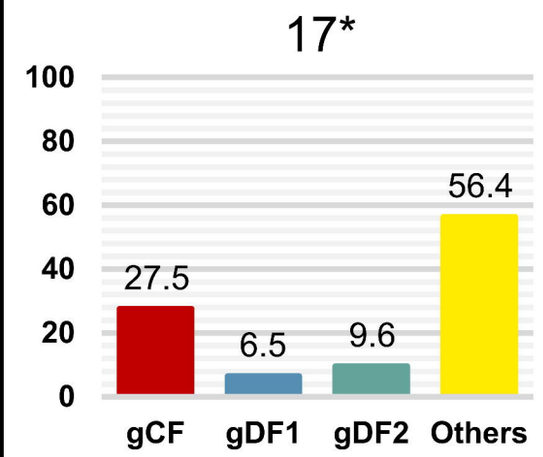

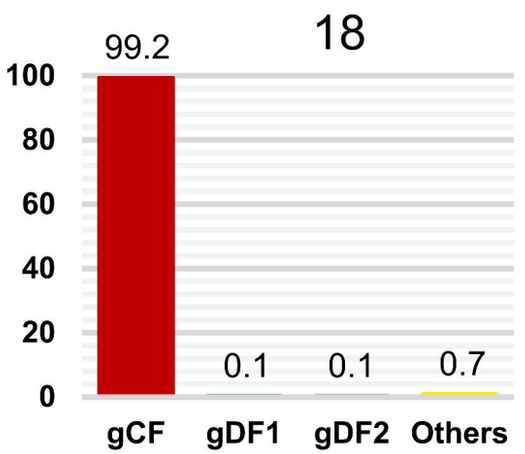

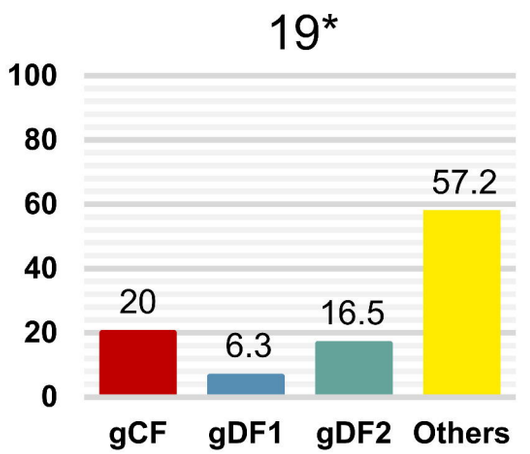

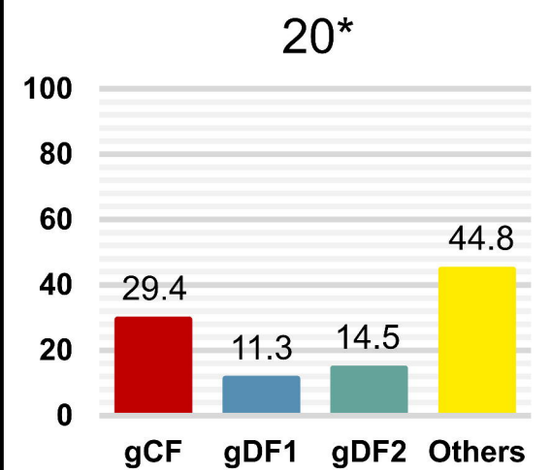

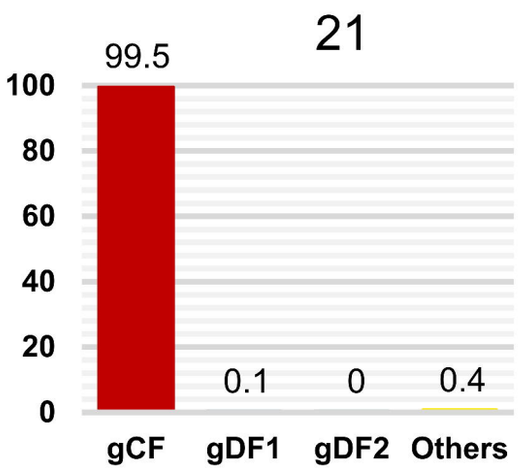

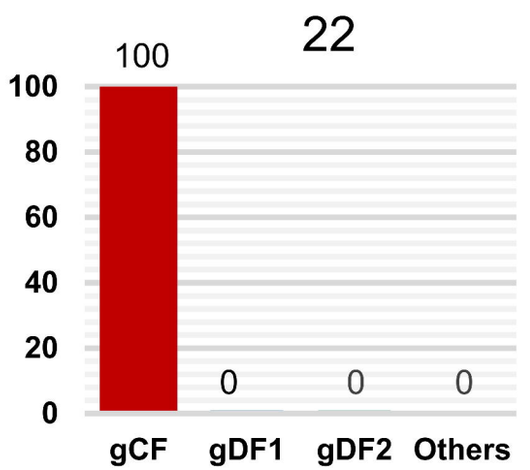

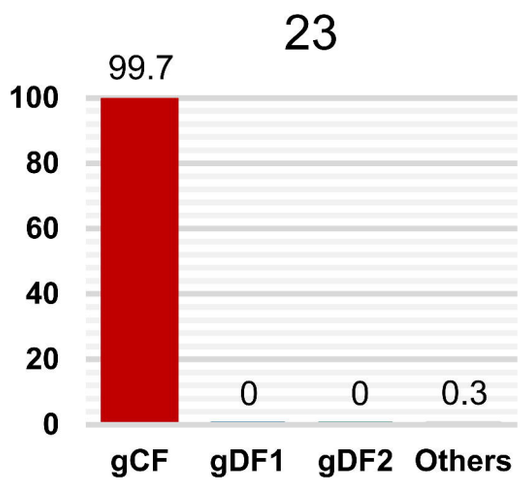

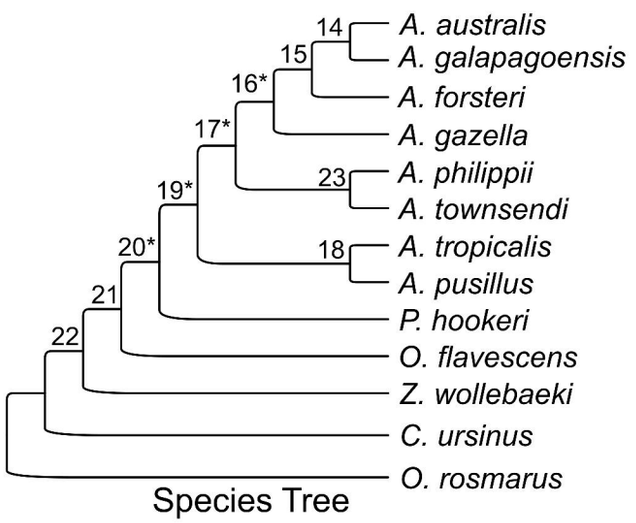

Introgression	Outgroup	mixprop1 ILS (%)	mixprop2 non-ILS (%)	Number of Trees	Total non-ILS (%)
Afor Aaus	Agal	5	95	706	12
Afor Agal	Aaus	8	92	559	9
Agal Aaus	Afor	3	97	4222	75
Atow Afor	Agaz	84	16	1610	0
Atow Agaz	Afor	70	30	1464	8
Agaz Afor	Atow	76	24	2413	11
Atow Agal	Agaz	96	4	1625	0
Atow Agaz	Agal	70	30	1451	8
Agaz Agal	Atow	78	22	2411	9
Atow Aaus	Agaz	92	8	1620	0
Atow Agaz	Aaus	70	30	1450	8
Agaz Aaus	Atow	77	23	2417	10
Aphi Afor	Agaz	85	15	1611	0
Aphi Agaz	Afor	69	31	1465	8
Agaz Afor	Aphi	77	23	2411	10
Aphi Agal	Agaz	97	3	1624	0
Aphi Agaz	Agal	69	31	1453	8
Agaz Agal	Aphi	80	20	2410	0
Aphi Aaus	Agaz	94	6	1621	0
Aphi Agaz	Aaus	69	31	1451	8
Agaz Aaus	Aphi	78	22	2415	10
Zwol Ejub	Zcal	79	21	1302	5
Zwol Zcal	Ejub	56	44	1385	11
Zcal Ejub	Zwol	61	39	2800	20